
PFN-TS: Thompson Sampling for Contextual Bandits via Prior-Data Fitted Networks

Yan Shuo Tan^{1*} Kenyon Ng² Ruizhe Deng¹

Sumetha Loganathan¹ Qiong Zhang³ Bibhas Chakraborty⁴

¹National University of Singapore ²Monash University

³Renmin University of China ⁴Duke-NUS Medical School

Abstract

Thompson sampling is a widely used strategy for contextual bandits: at each round, it samples a reward function from a Bayesian posterior and acts greedily under that sample. Prior-data fitted networks (PFNs), such as TabPFN v2+ and TabICL v2, are attractive candidates for this purpose because they approximate Bayesian posterior predictive distributions in a single forward pass. However, PFNs predict noisy future rewards, while Thompson sampling requires uncertainty over the latent mean reward function. We propose PFN-TS, a Thompson sampling algorithm that converts PFN posterior predictives into mean-reward samples using a subsampled predictive central limit theorem. The method estimates posterior variance from a geometric grid of $O(\log n)$ dataset prefixes rather than the full $O(n)$ predictive sequence used in previous predictive-sequence approaches, and reuses TabICL’s cached representations across rounds. We prove consistency of the subsampled variance estimator and give a Bayesian regret bound that decomposes PFN-TS regret into exact posterior-sampling regret under the PFN prior plus approximation terms. Empirically, PFN-TS achieves the best average rank across nonlinear synthetic and OpenML classification-to-bandit benchmarks, remains competitive on linear and BART-generated rewards, and attains the highest estimated policy value in an offline mobile-health evaluation. Code is available at https://anonymous.4open.science/r/PFN_TS-36ED/.

1 Introduction

Contextual bandits formalize sequential decision-making under uncertainty: at each round a learner observes a context, selects an action, and receives a stochastic reward, with the goal of minimizing cumulative regret over T rounds. Thompson Sampling (TS) [27, 24] addresses this by maintaining a Bayesian posterior over reward functions and sampling actions from it, but its performance is only as good as the underlying reward model. In tabular applications such as mobile health [15, 2] and recommendation systems [17], linear reward models [1] are standard yet often badly misspecified: human behavior involves interactions, threshold effects, and heterogeneity that linearity cannot capture. Richer alternatives—kernel methods [5], neural networks [32], and tree ensembles [21, 6]—each trade one limitation for another: kernel methods scale poorly in high dimensions, neural networks carry heavy computational overhead, and tree-based methods impose piecewise-constant structure that fits poorly in smooth or near-linear regimes. Compounding these model-specific weaknesses, all these approaches require hyperparameter choices, such as kernel bandwidth, network architecture, or tree depth, that are difficult to tune in an online setting.

*Correspondence: yanshuo@nus.edu.sg

Recently, tabular foundation models (TFMs) have emerged as state-of-the-art for regression and classification on small-to-medium tabular datasets. Among TFMs, TabPFN [14] and TabICLv2 [22] stand out because they are implemented as amortized Bayesian engines, also known as Prior-Data Fitted Networks (PFNs) [19]: They are trained to approximate the Bayesian posterior predictive distributions (PPDs) arising from a broad prior over data-generating processes. When deployed on a new dataset, they approximate the PPD via a single forward pass, without any parameter updates, a paradigm known as in-context learning (ICL). This broad prior and ICL approach confer three properties that are unusually well-suited to bandit deployment. First, *model-fitting is very fast* since it requires no parameter updates. Second, *no hyperparameter tuning* is required and yet these models outperform AutoML baselines on benchmark datasets. Third, the models exhibit *structural adaptivity*: because the prior covers a wide range of DGPs, predictions automatically reflect whichever structure (e.g. sparsity, smoothness, nonlinearity, or heteroscedasticity) is consistent with the observed data, avoiding the misspecification that afflicts single-model-class baselines [31]. Unfortunately, while these models output PPDs that quantify uncertainty in a noisy future response, they do not directly output posterior distributions for the latent regression function, which is what is needed by TS.

A potential solution comes from Bayesian predictive inference, which shows how to recover posterior parameter distributions from PPDs [8, 9]. One can either (i) sample from the posterior by recursively simulating future observations from a model’s PPDs, or (ii) estimate the posterior variance by tracking how much the PPDs fluctuate as we condition on prefixes of the observed data, thereby constructing a normal approximation. Ng et al. [20] and Fortini et al. [10] apply these respective techniques to calculate estimates of regression function posteriors for TabPFN in an offline setting. However, the cost of computing the full sequence of PPDs required to construct either method’s posterior estimates means that neither is practical for deployment in an online bandit setting, where a fresh posterior sample is needed for each arm at each round.

In this work, we break this computational bottleneck. Building on Fortini et al. [10], we construct a normal approximation to the posterior, but using a more efficient consistent variance estimator. More precisely, given an observed dataset of size n , we show that the asymptotic variance of the posterior can be consistently estimated using model snapshots along $O(\log n)$ geometrically spaced prefixes rather than all n prefixes. We embed this posterior approximation for PFNs into a TS framework, which we call *PFN-TS*. PFN-TS further reduces per-round cost by reusing cached representations of the fitted PFN across rounds. We derive a Bayesian regret bound for PFN-TS stated in terms of the maximum information gain for the Bayesian model defined by the broad prior and the error incurred by the PFN’s approximation of its PPD.

While our methodology and theory apply to any PFN, we instantiate our method with TabICLv2 [22] (hereafter TabICL), a PFN for tabular regression and classification that extends TabPFN [13, 14] with architectural improvements and, critically, caching of the key-value attention matrices for a fixed training set. In the bandit setting, where the same history is queried once per arm per round, this reduces the per-round cost substantially. We evaluate it against a comprehensive set of baselines on synthetic benchmarks, eight OpenML classification datasets, and the Drink Less mobile health trial, following the same experimental protocol as Deng et al. [6]. We find that PFN-TS substantially outperforms all baselines on almost all nonlinear tasks, while matching the performance of LinTS on linear tasks, and achieves the highest estimated policy value on the Drink Less trial.

2 Posterior Uncertainty from Predictive Sequences

2.1 PFNs as amortized Bayesian inference

Prior-Data Fitted Networks (PFNs) [19] are transformer models trained to approximate Bayesian PPDs in a single forward pass. To be precise, we define the following hierarchical Bayesian model:

$$\mathcal{D} \cup \{(x, y)\} \mid \pi, N \stackrel{\text{i.i.d.}}{\sim} \pi, \quad \pi \sim \Pi, \quad N \sim \rho_N, \quad (1)$$

where $\mathcal{D} = \{(x_i, y_i)\}_{i=1}^N$ is a dataset of random size N , π is a joint distribution over the pair (x, y) , Π is a prior over such distributions, and ρ_N is a distribution over dataset sizes. During training, synthetic datasets are drawn from this model, and the network minimizes negative log-likelihood given a training set and a query input. In other words, the network learns to approximate the mapping $(x, \mathcal{D}) \mapsto p(y|x, \mathcal{D})$, where $p(y|x, \mathcal{D}) = \int \pi(y|x)\Pi(\pi|\mathcal{D}) d\Pi(\pi)$ is the PPD.

2.2 Predictive sequences as posterior samplers

For a query point x and a dataset $\mathcal{D} = \{(x_i, y_i)\}_{i=1}^n$, define the sequence of predictive means $m_i(x) = m(x; \mathcal{D}_{1:i})$, $i = 0, \dots, n$, where $m(x; \mathcal{D})$ is the mean of the transformer’s output distribution at query x given context \mathcal{D} , and $\mathcal{D}_{1:i}$ is the first i observations in a fixed ordering of \mathcal{D} .

Exact PPD predictive sequences. In the idealized setting when the PFN is an exact Bayesian PPD for prior Π , we have $m_i(x) = \mathbb{E}_\Pi[y \mid x, \mathcal{D}_{1:i}]$, the posterior mean of the response at x given the first i observations. By the tower property, $\mathbb{E}[m_{i+1}(x) \mid \mathcal{F}_i] = m_i(x)$, so the sequence forms a Doob martingale with respect to the filtration $\mathcal{F}_i = \sigma(\mathcal{D}_{1:i})$ and, under regularity conditions, converges a.s. to a limit $m_\infty(x)$ by the Doob martingale convergence theorem.

To identify this limit, assume the data are i.i.d. draws from π (i.e., model (1) is correctly specified). As $n \rightarrow \infty$, the posterior $\Pi(\pi \mid \mathcal{D}_{1:n})$ concentrates on the true π a.s. (Bayesian consistency), so $p(y \mid x, \mathcal{D}_{1:n}) \rightarrow \pi(y \mid x)$ and hence $m_\infty(x) = f_0(x) := \int y \pi(y \mid x) dy$ a.s.

A crucial consequence is that the law of $m_\infty(x)$ given $\mathcal{D}_{1:n}$ coincides with the posterior over $f_0(x)$:

$$\mathcal{L}(m_\infty(x) \mid \mathcal{D}_{1:n}) = p(f_0(x) \mid \mathcal{D}_{1:n}). \quad (2)$$

This follows from the a.s. identity $m_\infty(x) = f_0(x)$. The randomness of $m_\infty(x)$ given $\mathcal{D}_{1:n}$ — which comes from the unobserved future data that would determine the limit — is exactly the Bayesian uncertainty about $f_0(x)$ [9]. Equivalently, the posterior uncertainty is the conditional law of the martingale tail $m_\infty(x) - m_n(x)$ given $\mathcal{D}_{1:n}$. Martingality gives the centering and orthogonality structure, but a Gaussian approximation requires second-order regularity of the predictive increments. Under predictive-CLT conditions, this tail satisfies

$$\mathcal{L}(\sqrt{n}(m_\infty(x) - m_n(x)) \mid \mathcal{D}_{1:n}) \xrightarrow{w} \mathcal{N}(0, V(x)) \quad \mathbb{P}\text{-a.s.}, \quad (3)$$

as $n \rightarrow \infty$, giving a tractable Gaussian approximation to the posterior over the latent mean $f_0(x)$ that can be used directly for Thompson sampling.

Approximate PPD predictive sequences. Since TabPFN and TabICL only provide an approximation to the exact PPD, the above properties do not hold automatically. Fong et al. [8] proved that under martingale conditions on the predictive sequence, the limit $m_\infty(x)$ still exists and is identifiable as a random variable, although not necessarily equal to $f_0(x)$. Calling it a martingale posterior, they argue that it still offers a form of uncertainty quantification, which can be computed by simulating future values in the predictive sequence.

Unfortunately, TabPFN and TabICL do not satisfy the exact martingale condition either. To address this issue, Ng et al. [20] and Fortini et al. [10] introduce more relaxed sufficient conditions on the predictive sequences that still guarantee the existence of a limiting random variable, and provide empirical evidence that TabPFN’s predictive sequences exhibit such limiting behavior, thereby enabling uncertainty quantification in an offline setting. While they worked with predictive CDFs rather than means, a similar analysis applies to the predictive mean sequence as well. We now state a similar set of assumptions for our setting, that we will use throughout the rest of the paper.

Assumption 1 (Asymptotic variance). *There $\exists V(x) > 0$ s.t. $i^2 \mathbb{E}[(m_i(x) - m_{i-1}(x))^2 \mid \mathcal{F}_{i-1}] \rightarrow V(x)$ a.s. as $i \rightarrow \infty$.*

Assumption 2 (Quasi-martingale condition). $\sum_{i \geq 1} \sqrt{i} \left(\mathbb{E} \left[\left(\mathbb{E}[m_i(x) - m_{i-1}(x) \mid \mathcal{F}_{i-1}] \right)^2 \right] \right)^{1/2} < \infty$.

Assumption 3 (Bounded moments). *There exist $C > 0$ and $\epsilon > 0$ such that $\mathbb{E}[(m_i(x) - m_{i-1}(x))^{4+\epsilon}] \leq C/i^{4+\epsilon}$.*

Following Fortini et al. [10, Theorem 4.3] and under these assumptions, one can establish a predictive CLT similar to (3) whose asymptotic variance $V(x)$ can be estimated by $\frac{1}{n} \sum_{i=1}^n i^2 (m_i(x) - m_{i-1}(x))^2$, but evaluating this requires a forward pass at all n dataset prefixes, which is prohibitive in an online bandit setting where a fresh variance estimate is needed for each arm at each round.

2.3 Subsampled CLT for predictive means

Rather than evaluating all n increments $m_i(x) - m_{i-1}(x)$, we compute block increments at $O(\log n)$ geometrically spaced prefix indices $2 = t_0 < t_1 < \dots < t_J \leq n$, where t_J is the last point in

the geometric sequence not exceeding n . For interval $(t_{j-1}, t_j]$, set $D_j = m_{t_j}(x) - m_{t_{j-1}}(x)$ and $w_j = t_j t_{j-1} / (t_j - t_{j-1})$.

To see why this weighting is natural, write each increment as a martingale-difference term plus a predictable drift. When the drift is negligible, martingale orthogonality suggests $\mathbb{E}[D_j^2] \approx V(x) \sum_{i=t_{j-1}+1}^{t_j} i^{-2} \approx V(x)(1/t_{j-1} - 1/t_j)$, so the harmonic weights w_j achieve the same identification target as the i^2 weights in the estimator of Fortini et al. [10] on a coarser grid.

The resulting variance estimator is

$$\hat{V}_{s_n}(x) = \frac{1}{J} \sum_{j=1}^J w_j D_j^2, \quad (4)$$

where $s_n = t_J$ is the latest refresh point. The cached sampler uses the snapshot Gaussian approximation $\mathcal{N}(m_{s_n}(x), \hat{V}_{s_n}(x)/s_n)$. With $J = O(\log_b n)$ terms, the default $b = 2$ requires $O(\log_2 n)$ forward passes per arm per round. Pseudocode is in Algorithm 1 (see also Figure 1); the formal guarantee is as follows.

Theorem 1 (Subsampled predictive CLT). *Under Assumptions 1 to 3,*

$$\mathcal{L}(\sqrt{q} (m_\infty(x) - m_q(x)) \mid \mathcal{D}_{1:q}) \xrightarrow{w} \mathcal{N}(0, V(x)) \quad \mathbb{P}\text{-a.s.}$$

as $q \rightarrow \infty$. Therefore the same CLT holds along any diverging sequence of refresh points. Moreover, for a history of size n and the geometric grid obtained by iterating $t_{j+1} = \max(t_j+1, \lfloor b t_j \rfloor)$ up to the last point $t_J \leq n$, with fixed $b > 1$, the estimator $\hat{V}_{s_n}(x)$ defined in Equation (4) satisfies $\hat{V}_{s_n}(x) \xrightarrow{P} V(x)$, where $s_n = t_J$.

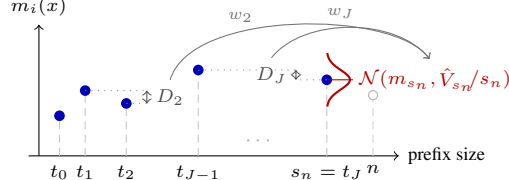


Figure 1: SubCLT evaluates the predictive mean on a geometric prefix grid. The trajectory increments D_j estimate the CLT variance used for the Thompson sample at the latest refresh point s_n .

3 Thompson Sampling with PFNs

3.1 Problem setup

We consider the standard contextual bandit over T rounds. At each round $t \in [T]$, the learner observes a context $X_t \in \mathcal{X} \subseteq [0, 1]^p$, selects an action $A_t \in \mathcal{A}$ where $|\mathcal{A}| = K$, and receives a reward

$$R_t = f_0(X_t, A_t) + \varepsilon_t, \quad (5)$$

where $f_0 : \mathcal{X} \times \mathcal{A} \rightarrow \mathbb{R}$ is the unknown mean reward function and ε_t is independent mean-zero noise with $|\varepsilon_t| \leq B$ almost surely. The history at round t is $\mathcal{H}_t = \{(X_s, A_s, R_s)\}_{s=1}^t$. The goal is to minimize cumulative regret against the oracle policy $A^*(x) \in \arg \max_{a \in \mathcal{A}} f_0(x, a)$:

$$\text{Regret}_T = \sum_{t=1}^T (f_0(X_t, A^*(X_t)) - f_0(X_t, A_t)).$$

Thompson Sampling maintains a posterior $\Pi(\cdot \mid \mathcal{H}_{t-1})$ over reward functions and at each round draws $\hat{f}_t \sim \Pi(\cdot \mid \mathcal{H}_{t-1})$ and plays $A_t = \arg \max_a \hat{f}_t(X_t, a)$.

3.2 Context parameterization

A design choice in applying any tabular model to contextual bandits is how to represent arm identity in the input. We consider two strategies.

Disjoint encoding maintains K independent models, one per arm. For arm k , the history is $\mathcal{D}^{(k)} = \{(X_s, R_s) : s \leq t, A_s = k\}$, and the predictive mean at query X_t is $m(X_t; \mathcal{D}^{(k)})$. Each model sees only the data from its own arm.

Joint encoding (one-hot) maintains a single model with arm identity appended as a one-hot vector: the feature for arm k and context x is $\tilde{x}_k = (x, e_k) \in \mathbb{R}^{p+K}$, where $e_k \in \{0, 1\}^K$. The joint history

$\mathcal{D}^t = \{(\tilde{X}_{s,A_s}, R_s) : s \leq t\}$ is used for all arms. This allows observations from one arm to inform predictions for another.

Neither encoding universally dominates. Joint encoding is preferable when arms share structure, since it pools observations; disjoint encoding is more effective when arm reward functions are unrelated. A third option, *block encoding*, expands the feature space to \mathbb{R}^{pK} by placing x in the k -th block and zero-padding elsewhere, but the K -fold increase in dimensionality makes it less practical for PFNs.

3.3 The PFN-TS algorithm

After a round-robin warm-up of τ observations per arm, PFN-TS enters its main Thompson Sampling loop. We describe how it operates under each encoding, then explain the adaptive selection rule.

Disjoint encoding. Each arm k maintains its own model and history $\mathcal{D}^{(k)}$ of size $n_k = |\mathcal{D}^{(k)}|$. At each round t , SUBCLT is called with $\mathcal{D}^{(k)}$ and query X_t , evaluating the predictive mean at a geometrically spaced grid $t_0 < t_1 < \dots < t_J \leq n_k$ of prefix sizes. These grid points are the *refresh times* for arm k : at each t_j , the KV cache for prefix $\mathcal{D}_{1:t_j}^{(k)}$ is stored for reuse in subsequent rounds. Let $s_{t,k} = t_J$ be the latest refresh point for arm k . The Thompson sample is drawn from the snapshot Gaussian approximation

$$\tilde{r}_{t,k} \sim \mathcal{N}\left(m(X_t; \mathcal{D}_{1:s_{t,k}}^{(k)}), \hat{V}_{s_{t,k}}(X_t)/s_{t,k}\right).$$

The arm with the highest sample is selected: $A_t = \arg \max_k \tilde{r}_{t,k}$.

Joint encoding. Under joint encoding the setup is similar, but with a single shared model and history \mathcal{D} of size $n = |\mathcal{D}|$, queried at the augmented context (X_t, e_k) for each arm k . The refresh times $t_0 < t_1 < \dots < t_J \leq n$ are now based on the *total* history and shared across arms: at each t_j , the KV cache for prefix $\mathcal{D}_{1:t_j}$ is built once and reused for all K arm queries, reducing the per-round SubCLT cost from $O(K \log n_k)$ to $O(\log n)$. Since the variance estimate is computed at the latest shared refresh point $s_t = t_J$, the Thompson sample uses the shared snapshot size:

$$\tilde{r}_{t,k} \sim \mathcal{N}\left(m((X_t, e_k); \mathcal{D}_{1:s_t}), \hat{V}_{s_t}(X_t, e_k)/s_t\right)^2.$$

Adaptive encoding selection. Since neither encoding dominates in general, PFN-TS runs both in parallel during a *dual-encoding* phase and selects between them via the Continuous Ranked Probability Score (CRPS) [11]: for a predictive CDF \hat{F} and outcome r ,

$$\text{CRPS}(\hat{F}, r) = \int_{-\infty}^{\infty} (\hat{F}(y) - \mathbf{1}\{y \geq r\})^2 dy. \quad (6)$$

CRPS is a strictly proper scoring rule, so the better-calibrated encoding accumulates lower cumulative CRPS. At pre-specified *switch times* $S = \{s_1 < \dots < s_L\}$, cumulative CRPS is compared and the better encoding becomes active; after s_L , the challenger is discarded. Snapshot caching at refresh times means CRPS evaluation requires no additional forward passes: observations since the last switch are replayed against the stored snapshots. Full pseudocode is in Algorithm 2 (Section B).

Related work. Zhang et al. [30] propose a closely related framework in which TS uncertainty is recast as arising from missing counterfactual outcomes: a generative sequence model, pretrained on bandit data from previous tasks, imputes all unobserved arm outcomes at each round, and a policy is then fit on the imputed complete dataset. Relative to their approach, ours differs in three ways: (i) we use a generic PFN without any task-specific training; (ii) we extract uncertainty from the predictive distribution directly via SubCLT rather than by generating counterfactual outcomes for all arms, avoiding the cost of full imputation passes; and (iii) we operate in the single-task setting without requiring offline data from previous tasks in the same distribution.

4 Bayesian Regret of PFN-TS

To bound the Bayesian regret of PFN-TS, we compare it to exact Thompson Sampling in the Bayesian model associated with the prior Π . The regret analysis uses the disjoint-arm Bayesian design induced

²For joint encoding, a fully Bayesian Thompson sampler would sample the arm-reward vector jointly from the predictive law induced by the shared context. Our implementation samples independently from marginal Gaussian approximations, so the joint-encoding variant should be viewed as a heuristic empirical extension of the disjoint sampler.

by (1): for each arm a , an independent joint law $\pi_a \sim \Pi_a$ is drawn, with common context marginal on \mathcal{X} , and rewards queried at arm a are generated from the conditional law $\pi_a(\cdot | x)$. Thus the prior over mean reward functions is $\Pi = \bigotimes_{a=1}^K \Pi_a$, where $f_0(x, a) = \int y \pi_a(dy | x)$. Contexts are exogenous draws from the common context marginal. Conditional on the realized contexts and selected actions, the posterior update for arm a is the arm-specific posterior predictive update from (1) restricted to the observed pairs in $\mathcal{D}^{(a)}$; adaptivity enters only through which contexts are queried for each arm. Under this Bayesian design, regret is

$$\mathbb{E}[\text{Regret}_T] = \mathbb{E} \left[\sum_{t=1}^T (f_0(X_t, A_t^*) - f_0(X_t, A_t)) \right],$$

with expectation over the prior, contexts, rewards, and algorithmic randomness. The result is stated for disjoint encoding. Under joint encoding, the transformed contexts need not arise from arm-specific copies of (1), so the same argument does not directly apply.

Let $P_t^\Pi(\cdot | x, \mathcal{D}^{(1:K)})$ be the action distribution induced by exact posterior sampling under Π after context x and arm histories $\mathcal{D}^{(1:K)} = (\mathcal{D}^{(1)}, \dots, \mathcal{D}^{(K)})$. Let $Q_t(\cdot | x, \mathcal{D}^{(1:K)})$ be the corresponding action distribution used by PFN-TS.

Theorem 2 (Bayesian regret with sampler approximation). *Suppose the posterior expected reward range is uniformly bounded by a finite constant $2B_R$: for every finite arm-specific history collection $\mathcal{D}^{(1:K)}$,*

$$\sup_{x \in \mathcal{X}, a, a' \in \mathcal{A}} \mathbb{E}_\Pi \left[|f_0(x, a) - f_0(x, a')| \mid \mathcal{D}^{(1:K)} \right] \leq 2B_R.$$

Then

$$\mathbb{E}[\text{Regret}_T^{\text{PFN}}] \leq \mathbb{E}[\text{Regret}_T^{\Pi\text{-TS}}] + 2B_R \sum_{t=1}^T (T - t + 1) \varepsilon_t.$$

Here $\text{Regret}_T^{\Pi\text{-TS}}$ is the regret of exact Thompson Sampling under Π and

$$\varepsilon_t = \sup_{x, \mathcal{D}^{(1:K)}} \text{TV} \left(Q_t(\cdot | x, \mathcal{D}^{(1:K)}), P_t^\Pi(\cdot | x, \mathcal{D}^{(1:K)}) \right).$$

The theorem is a coupling statement. If PFN-TS and exact Π -TS have the same history at round t , a maximal coupling makes their actions differ with probability at most ε_t . Once their actions differ, their future histories may differ, which produces the factor $T - t + 1$. The first term is the regret of the ideal Bayesian algorithm for the prior approximated by TabICL; the second term measures the cost of using the PFN-TS sampler instead of exact posterior sampling.

Remark 1 (Bounding the exact Bayesian term). *The regret of exact Π -TS can be bounded using the standard information-ratio framework. Under disjoint encoding and a product prior, the factorization argument of Deng et al. [6] gives*

$$\mathbb{E}[\text{Regret}_T^{\Pi\text{-TS}}] \leq \sqrt{2T \bar{\Gamma}_T(\Pi) \gamma_T(\Pi)}.$$

Here $\bar{\Gamma}_T(\Pi)$ is the worst-case information ratio of exact Π -TS, and $\gamma_T(\Pi)$ is the corresponding disjoint maximum information gain. If posterior reward distributions under Π are uniformly sub-Gaussian with proxy σ_R^2 , then finite-action Thompson Sampling bounds suggest $\bar{\Gamma}_T(\Pi) \lesssim K \sigma_R^2$ [12]. The term $\gamma_T(\Pi)$ depends on the complexity of the prior Π ; Section A.2 gives the formal definition and comparison rates for linear and Hölder classes.

Remark 2 (Bounding the sampler error). *Theorem 3 bounds ε_t by a Gaussian approximation error for exact posterior sampling under Π plus a KL-type discrepancy between the Gaussian from exact-PPD SubCLT and that constructed from applying SubCLT to the PFN's PPD approximations. The latter term depends on predictive mean error and the induced variance ratio, so the coupling error is controlled by approximation properties of the PFN.*

5 Numerical Experiments

Across synthetic and real-data benchmarks, PFN-TS improves over standard baselines when reward functions are nonlinear or heterogeneous, while remaining competitive on problems where simpler

Table 1: Final cumulative regret on synthetic benchmarks (mean \pm SE, $T = 10,000$, $R = 5$ replications). **Bold**: lowest mean per scenario; avg rank computed across all scenarios.

Method	Friedman	Friedman-Hetero.	Friedman-Sparse	Friedman-Sparse-Dis.	Friedman2	Friedman3	Linear	SynBART	Rank
PFN-TS (ours)	233.0 \pm 94.1	243.2 \pm 67.4	306.3 \pm 78.5	568.6 \pm 57.5	90.2 \pm 21.3	136.4 \pm 14.6	261.4 \pm 81.5	51.2 \pm 31.0	1.375
BFTS	680.3 \pm 98.5	777.1 \pm 126.6	835.5 \pm 91.6	684.4 \pm 66.1	367.1 \pm 74.3	559.3 \pm 67.8	570.4 \pm 212.5	50.9 \pm 20.0	2.375
LinearTS	15690.6 \pm 12812.3	26214.7 \pm 149.0	10427.3 \pm 12770.9	6529.8 \pm 1210.7	524.8 \pm 168.8	5260.7 \pm 10521.5	66.9 \pm 14.1	301.1 \pm 76.0	5.125
LinearUCB	26222.5 \pm 215.8	26214.7 \pm 149.0	23106.6 \pm 6305.4	7743.7 \pm 2746.3	682.1 \pm 120.2	26304.4 \pm 244.2	79.2 \pm 21.2	274.0 \pm 113.1	6.000
NeuralTS	5697.3 \pm 10349.9	20311.5 \pm 10242.4	9673.3 \pm 9809.5	1376.3 \pm 151.2	148.2 \pm 114.0	728.6 \pm 905.3	520.7 \pm 234.5	198.2 \pm 73.4	4.000
RFTS	2504.5 \pm 139.0	2562.1 \pm 218.8	2688.8 \pm 259.4	7579.2 \pm 218.9	1058.4 \pm 85.2	909.6 \pm 123.5	781.7 \pm 297.2	106.7 \pm 47.7	4.875
XGBoostTS	2354.4 \pm 115.4	2432.1 \pm 119.8	2694.1 \pm 82.4	4962.3 \pm 133.1	780.9 \pm 33.5	1738.6 \pm 49.3	704.9 \pm 283.6	66.7 \pm 28.3	4.250

inductive biases are well matched to the data. Figure 2 shows selected regret curves; full trajectories are in Sections D.1 and D.3.

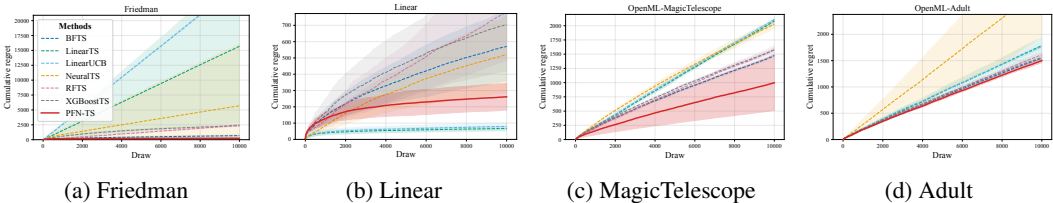


Figure 2: Selected cumulative regret trajectories (mean \pm SD, $R = 5$ replications, $T = 10,000$). Left to right: Friedman (synthetic), Linear (synthetic), MagicTelescope (OpenML), Adult (OpenML). Full results are in Sections D.1 and D.3.

5.1 Experimental Setup

We compare PFN-TS with **LinTS** (linear Thompson Sampling), **LinUCB** [17], **NeuralTS** [32], **BFTS** [6], **RFTS**, and **XGBoostTS** [21]. The baseline implementations and fixed settings follow Deng et al. [6], with the method-specific choices listed in Section C.4. Synthetic and OpenML experiments use horizon $T = 10,000$ and $R = 5$ independent replications. PFN-TS uses geometric base $b = 2$, no context-window truncation, and a warm-up of $\tau = 5$ round-robin pulls per arm; BFTS uses the same warm-up convention. LinTS and NeuralTS are tuned on a separate pilot run, while the other baselines use fixed settings.

5.2 Synthetic Benchmarks

We evaluate on three families of data-generating processes (DGPs): (i) **Linear** rewards with Gaussian noise, (ii) **Friedman** nonlinear rewards with varying sparsity, correlation structure, and heteroscedastic noise, and (iii) **SynBART**, where each arm’s reward function is sampled from a BART prior, providing a correctly-specified benchmark for BFTS. Full DGP definitions are in Section C.1.

Table 1 reports final cumulative regret across all scenarios. PFN-TS has the best average rank overall (1.38) and achieves the lowest regret on all six Friedman variants, often by a large margin over tree and neural baselines. The main exceptions align with model specification: LinTS is best on the Linear benchmark, while BFTS narrowly edges PFN-TS on SynBART, where the reward functions are drawn from the BART prior used by BFTS. The selected trajectories in Figure 2 illustrate this pattern: PFN-TS separates quickly on nonlinear Friedman rewards, while LinTS remains the right inductive bias on the linear task.

SubCLT uncertainty diagnostics. To isolate uncertainty quality from adaptive data collection, we also evaluate SubCLT in offline regression experiments. For Linear and Friedman DGPs, we fit on $n \in \{16, 64, 256, 1024\}$ observations, construct nominal 95% intervals for the latent mean at held-out queries, and plot empirical coverage against mean interval length. BART serves as an MCMC posterior baseline. Figure 3 shows a mixed but useful diagnostic: TabICL-SubCLT undercovers on the Linear DGP, but on the nonlinear Friedman DGP it attains near-nominal coverage with substantially shorter intervals than BART. Details are in Section D.2.

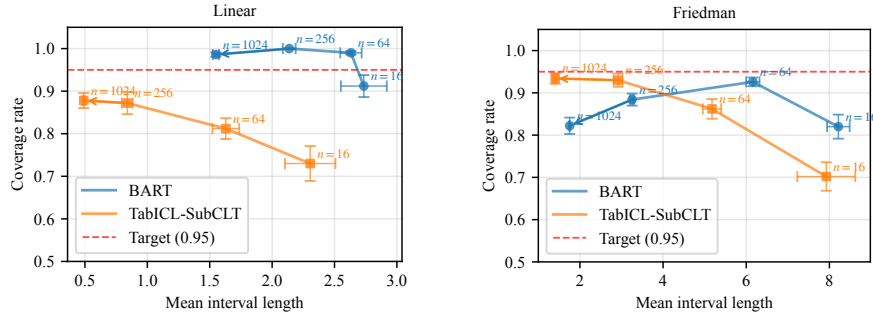


Figure 3: Coverage-length diagnostics for nominal 95% intervals. Each marker is one sample size; lower interval length at fixed coverage is better.

Table 2: Final cumulative regret on OpenML benchmarks (mean \pm SE). The rightmost column reports average rank across all eight datasets; lower is better.

Method	Adult	Covertype	EEGEyeState	GasDrift	MagicTelescope	Mushroom	PageBlocks	Shuttle	Rank
PFN-TS (ours)	1499.2 \pm 35.0	3441.0 \pm 457.7	625.6 \pm 12.7	350.8 \pm 32.3	998.0 \pm 486.6	37.0 \pm 4.8	295.6 \pm 16.2	681.4 \pm 572.3	1.875
BFTS	1548.8 \pm 44.1	3642.0 \pm 36.2	2270.6 \pm 37.6	878.8 \pm 59.6	1476.6 \pm 20.1	56.0 \pm 9.0	272.0 \pm 17.1	108.2 \pm 4.9	2.375
LinearTS	1785.0 \pm 150.4	3457.8 \pm 99.2	3649.2 \pm 50.8	489.2 \pm 11.1	2083.0 \pm 27.2	493.8 \pm 93.1	351.4 \pm 14.9	639.6 \pm 19.6	4.750
LinearUCB	1768.2 \pm 30.8	3705.2 \pm 52.2	3622.8 \pm 10.3	930.8 \pm 23.2	2110.0 \pm 23.6	401.4 \pm 3.4	370.4 \pm 16.5	767.8 \pm 43.1	5.625
NeuralTS	2984.8 \pm 1017.6	5014.8 \pm 1268.8	4977.6 \pm 38.7	7662.6 \pm 182.1	2031.0 \pm 74.5	1711.8 \pm 1924.3	412.4 \pm 24.2	429.0 \pm 332.5	6.375
RFTS	1614.4 \pm 41.7	3601.8 \pm 57.3	2666.0 \pm 66.7	2119.4 \pm 356.5	1577.8 \pm 71.0	69.6 \pm 26.6	292.6 \pm 19.4	176.6 \pm 42.6	3.500
XGBoostTS	1560.2 \pm 40.1	3535.2 \pm 82.8	2113.2 \pm 36.1	1215.4 \pm 32.2	1579.2 \pm 29.7	81.4 \pm 6.4	306.2 \pm 12.4	182.6 \pm 93.2	3.500

5.3 OpenML Benchmarks

We transform eight OpenML [29] classification tasks into contextual bandit problems following standard protocol [23, 32, 21, 6]: each class label becomes an arm, and the reward is 1 for choosing the correct class and 0 otherwise. We use Adult, Covertype, EEGEyeState, GasDrift, MagicTelescope, Mushroom, PageBlocks, and Shuttle.

Table 2 reports final cumulative regret and average rank across all eight datasets. PFN-TS again has the best average rank (1.88) and obtains the lowest final regret on six of the eight tasks: Adult, Covertype, EEGEyeState, GasDrift, MagicTelescope, and Mushroom. BFTS performs best on PageBlocks and Shuttle. Some representative OpenML trajectories are shown in Figure 2, with full per-dataset results in Section D.3. We note that the only OpenML dataset where PFN-TS is far from the best is Shuttle, which has a large number of arms (7) and a highly imbalanced reward structure. PFN-TS is less stable on this dataset, which we believe can be mitigated by further tuning of the encoding strategy; we leave this to future work.

5.4 Off-policy Evaluation: Drink Less mHealth Trial

To assess performance on real-world logged data, we apply PFN-TS to the Drink Less micro-randomized trial [2], a 30-day study in which $n = 349$ participants at risk of hazardous drinking were randomized daily among three push-notification actions (no message, standard message, tailored message) with static propensities (0.4, 0.3, 0.3). The reward is a binary proximal engagement indicator (app opening within the following hour). Following Deng et al. [6], we unfold the panel into $T = n \times 30 = 10,470$ sequential decision points, preserving within-participant temporal order, and simulate each algorithm’s policy in offline replay. Policy value is estimated using self-normalized importance sampling (SNIPS; Swaminathan and Joachims [26]), with a doubly-robust (DR) estimator as a robustness check [7]. Figure 4 shows that PFN-TS has the highest estimated SNIPS value by the final horizon, but performs worse than BFTS on shorter horizons. OPE diagnostics (importance weight distributions and DR estimates) are in Section D.4.

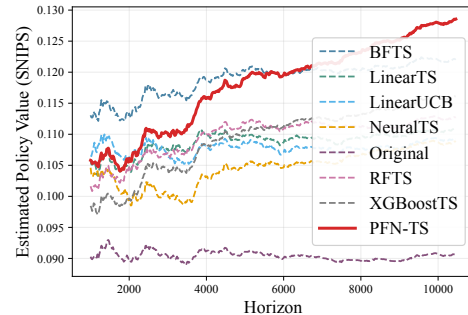


Figure 4: Estimated policy value (SNIPS) on the Drink Less trial. Higher is better.

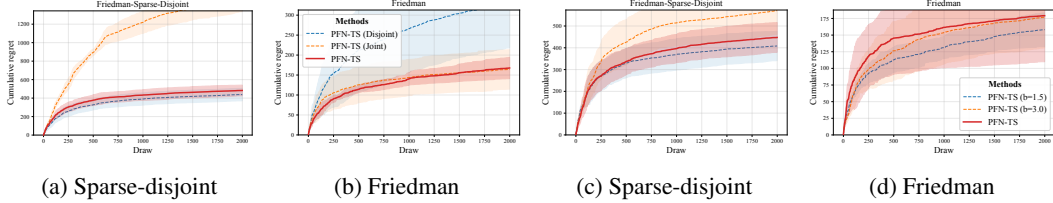


Figure 5: Selected ablations on two representative nonlinear DGPs (mean cumulative regret, $R = 5$ replications). The first two panels vary the arm encoding, comparing the adaptive rule with fixed disjoint and joint encodings; the last two panels vary the geometric subsampling base $b \in \{1.5, 2, 3\}$.

5.5 Ablation Studies

We examine three design choices of PFN-TS; full ablation plots are in Section D.5.

Encoding strategy. We compare the adaptive encoding rule (Section 3) against two fixed alternatives: *Disjoint* (separate context per arm, no arm indicator) and *Joint* (arm index appended to context as a categorical feature). Cumulative regret is sensitive to this choice: disjoint encoding is poor when arms share structure, while joint encoding can be less effective when arm-specific histories should remain separate. Figure 5 (left) shows that the adaptive rule is competitive with the better fixed encoding on both a shared-structure Friedman benchmark and a sparse disjoint-arm variant.

Subsampling grid. We vary the geometric base $b \in \{1.5, 2, 3\}$. Figure 5 (right) shows that smaller bases can modestly improve regret on some scenarios by using a denser prefix grid, but they require more forward passes. The default $b = 2$ gives a stable middle ground, with regret curves generally of the same order as the neighboring choices while using half as many CLT forward passes as $b = 1.5$.

Decision rule. We compare Thompson sampling (the default) against *PFN-PS* (sampling from the posterior predictive distribution) and *PFN-Greedy* (selecting the arm with the highest predictive mean). PFN-PS performs substantially worse, confirming that sampling noisy future rewards from the PPD is not a substitute for sampling latent mean rewards. Greedy selection can be competitive when the reward landscape is identified quickly, but PFN-TS retains an edge on harder tasks.

6 Discussion

PFN-TS shows that tabular in-context learning can serve as an effective reward model for sequential decision-making once efficient uncertainty extraction and adaptive encoding are in place.

Computation. Runtime is the main current limitation: SubCLT reduces uncertainty-estimation cost, but each decision still requires repeated TabICL evaluations across arms and grid points. Preliminary experiments suggest that reducing TabICL’s ensemble size from $n_{\text{estimators}} = 8$ to 1 substantially improves wall-clock time without noticeably changing regret, and low GPU utilization suggests room for batching, data-loading, and inference optimizations.

Finite-sample calibration. SubCLT is asymptotic and can be poorly calibrated when arm histories are short or weakly informative, as in the small- n coverage diagnostics, early Drink Less horizons, and Shuttle, where most arms observe zero rewards for many rounds. Regularized variants, such as shrinkage toward pooled variances, adaptive variance floors, or prior-informed pseudo-observations, are a natural next step.

Extensions. Posterior contraction or information-gain bounds for the TabPFN/TabICL prior would sharpen our Bayesian regret guarantee and could imply frequentist regret bounds. The adaptive encoding rule is empirical, large or infinite action spaces would require candidate generation or action search, and SubCLT-style uncertainty estimates may also be useful in active learning, adaptive experimentation, and online model selection with tabular foundation models.

Deployment. PFN-TS should not be deployed in high-stakes adaptive decision systems without application-specific validation. In settings such as mobile health, posterior uncertainty can improve exploration, but policies should be monitored for subgroup performance, safety constraints, and feedback loops induced by adaptive data collection.

Acknowledgments and Disclosure of Funding

QZ is supported by the National Key R&D Program of China Grant 2024YFA1015800. BC is supported by MOE Tier 2 grant MOE-T2EP20122-0013. YT is supported by NUS Start-up Grant A-8000448-00-00 and MOE AcRF Tier 1 Grant A-8002498-00-00. Additionally, BC and YT are supported by MOE AcRF Tier 1 Grant A-8004458-00-00.

References

- [1] Shipra Agrawal and Navin Goyal. Thompson sampling for contextual bandits with linear payoffs. In *International Conference on Machine Learning*, pages 127–135, 2013.
- [2] Lorraine Bell, Claire Garnett, Tianchen Qian, Lorraine Sherr, Felix Greaves, and Susan Michie. Drink less: Development and feasibility of a smartphone app for self-management of alcohol consumption. *JMIR mHealth and uHealth*, 8(5):e17049, 2020.
- [3] Patrizia Berti, Irene Crimaldi, Luca Pratelli, and Pietro Rigo. A central limit theorem and its applications to multicolor randomly reinforced urns. *Journal of Applied Probability*, 48(2):527 – 546, 2011. doi: 10.1239/jap/1308662642. URL <https://doi.org/10.1239/jap/1308662642>.
- [4] Hugh A Chipman, Edward I George, and Robert E McCulloch. BART: Bayesian additive regression trees. *Annals of Applied Statistics*, 4(1):266–298, 2010.
- [5] Sayak Ray Chowdhury and Aditya Gopalan. On kernelized multi-armed bandits. In *International Conference on Machine Learning*, pages 844–853, 2017.
- [6] Ruizhe Deng, Bibhas Chakraborty, Ran Chen, and Yan Shuo Tan. BFTS: Thompson sampling with bayesian additive regression trees. *arXiv preprint arXiv:2602.07767*, 2026.
- [7] Miroslav Dudík, John Langford, and Lihong Li. Doubly robust policy evaluation and learning. In *Proceedings of the 28th International Conference on International Conference on Machine Learning*, pages 1097–1104, 2011.
- [8] Edwin Fong, Chris Holmes, and Stephen G Walker. Martingale posteriors. *Journal of the Royal Statistical Society: Series B*, 85(5):1357–1391, 2023.
- [9] Sandra Fortini and Sonia Petrone. Exchangeability, Prediction and Predictive Modeling in Bayesian Statistics. *Statistical Science*, 40(1):40 – 67, 2025. doi: 10.1214/24-STS965. URL <https://doi.org/10.1214/24-STS965>.
- [10] Sandra Fortini, Kenyon Ng, Sonia Petrone, Judith Rousseau, and Susan Wei. A principled framework for uncertainty decomposition in TabPFN. *arXiv preprint*, 2026.
- [11] Tilmann Gneiting and Adrian E Raftery. Strictly proper scoring rules, prediction, and estimation. *Journal of the American Statistical Association*, 102(477):359–378, 2007.
- [12] Albin Gouverneur, Borja Rodriguez-Galvez, Lucas Theis, and Flavio P Calmon. Thompson sampling with less exploration is fast and optimal. In *International Conference on Machine Learning*, 2023.
- [13] Noah Hollmann, Samuel Müller, Katharina Eggenberger, and Frank Hutter. TabPFN: A transformer that solves small tabular classification problems in a second. In *International Conference on Learning Representations*, 2023.
- [14] Noah Hollmann, Samuel Müller, Lennart Purucker, Arjun Krishnakumar, Max Körfer, Shi Bin Hoo, Robin Tibor Schirmer, and Frank Hutter. Accurate predictions on small data with a tabular foundation model. *Nature*, 637(8045):319–326, 2025.
- [15] Predrag Klasnja, Lena Mamykina, Julio Jauregui, Joshua M Smyth, and Richard L Kravitz. Microrandomized trials: An experimental design for developing just-in-time adaptive interventions. *Health Psychology*, 34(S):1220–1228, 2015.
- [16] Andreas Krause and Cheng Soon Ong. Contextual Gaussian process bandit optimization. In *Advances in Neural Information Processing Systems*, volume 24, 2011.
- [17] Lihong Li, Wei Chu, John Langford, and Robert E Schapire. A contextual-bandit approach to personalized news article recommendation. In *Proceedings of the 19th International Conference on World Wide Web*, pages 661–670, 2010.

- [18] Lihong Li, Wei Chu, John Langford, and Xuanhui Wang. Unbiased offline evaluation of contextual-bandit-based news article recommendation algorithms. In *Proceedings of the fourth ACM international conference on Web search and data mining, WSDM '11*, pages 297–306, New York, NY, USA, February 2011. Association for Computing Machinery. ISBN 978-1-4503-0493-1. doi: 10.1145/1935826.1935878. URL <https://dl.acm.org/doi/10.1145/1935826.1935878>.
- [19] Samuel Müller, Noah Hollmann, Sebastian Pineda Arango, Josif Grabocka, and Frank Hutter. Transformers can do Bayesian inference. In *International Conference on Learning Representations*, 2022.
- [20] Kenyon Ng, Edwin Fong, David T Frazier, Jeremias Knoblauch, and Susan Wei. Tabmgrp: Martingale posterior with tabpfn. *arXiv preprint arXiv:2510.25154*, 2025.
- [21] Hannes Nilsson, Rikard Johansson, Niklas Åkerblom, and Morteza Haghir Chehreghani. Tree ensembles for contextual bandits. *Transactions on Machine Learning Research*, 2024. ISSN 2835-8856. URL <https://openreview.net/forum?id=59DCkSGw8S>.
- [22] Jingang Qu, David Holzmüller, Gaël Varoquaux, and Marine Le Morvan. Tabicl2: A better, faster, scalable, and open tabular foundation model. *arXiv preprint arXiv:2602.11139*, 2026.
- [23] Carlos Riquelme, George Tucker, and Jasper Snoek. Deep bayesian bandits showdown: An empirical comparison of bayesian deep networks for thompson sampling. In *International Conference on Learning Representations*, 2018. URL <https://openreview.net/forum?id=SyYe6k-CW>.
- [24] Daniel Russo and Benjamin Van Roy. An information-theoretic analysis of Thompson sampling. *Journal of Machine Learning Research*, 17(1):2442–2471, 2016.
- [25] Daniel J Russo, Benjamin Van Roy, Abbas Kazerouni, Ian Osband, and Zheng Wen. A tutorial on Thompson sampling. *Foundations and Trends in Machine Learning*, 11(1):1–96, 2018.
- [26] Adith Swaminathan and Thorsten Joachims. The self-normalized estimator for counterfactual learning. *Advances in Neural Information Processing Systems*, 28, 2015.
- [27] William R Thompson. On the likelihood that one unknown probability exceeds another in view of the evidence of two samples. *Biometrika*, 25(3/4):285–294, 1933.
- [28] Sattar Vakili, Kia Khezeli, and Victor Picheny. On information gain and regret bounds in Gaussian process bandits. In *International Conference on Artificial Intelligence and Statistics*, pages 82–90, 2021.
- [29] Joaquin Vanschoren, Jan N. Van Rijn, Bernd Bischl, and Luis Torgo. OpenML: networked science in machine learning. *ACM SIGKDD Explorations Newsletter*, 15(2):49–60, June 2014. ISSN 1931-0145, 1931-0153. doi: 10.1145/2641190.2641198. URL <https://dl.acm.org/doi/10.1145/2641190.2641198>.
- [30] Kelly W. Zhang, Tiffany Cai, Hongseok Namkoong, and Daniel Russo. Contextual thompson sampling via generation of missing data. In *The Thirty-ninth Annual Conference on Neural Information Processing Systems*, 2026. URL <https://openreview.net/forum?id=Fqs19IbfJ>.
- [31] Qiong Zhang, Yan Shuo Tan, Qinglong Tian, and Pengfei Li. TabPFN: One model to rule them all? *arXiv preprint arXiv:2505.20003*, 2025.
- [32] Weitong Zhang, Dongruo Zhou, Lihong Li, and Quanquan Gu. Neural thompson sampling. In *International Conference on Learning Representations*, 2021. URL <https://openreview.net/forum?id=tkAtoZkcUmm>.

A Proofs

A.1 Proof of Theorem 1

Proof. Write $\delta_i = m_i(x) - m_{i-1}(x)$ and decompose each increment as

$$\delta_i = \zeta_i + \xi_i,$$

where $\zeta_i = \delta_i - \mathbb{E}[\delta_i \mid \mathcal{F}_{i-1}]$ is the martingale-difference part and $\xi_i = \mathbb{E}[\delta_i \mid \mathcal{F}_{i-1}]$ is the conditional-mean (bias) part.

Part 1: CLT for $\sqrt{n}(m_\infty(x) - m_n(x))$.

We apply the quasi-martingale CLT of Berti et al. [3] (Proposition 1, restated as Theorem G.4 in Fortini et al. [10]) to the scalar sequence $(m_n(x))$. We verify its four requirements.

(UI) *Uniform integrability of $(m_n(x))$.* By conditional Jensen, $\mathbb{E}[\delta_i^2 \mid \mathcal{F}_{i-1}]^2 \leq \mathbb{E}[\delta_i^4 \mid \mathcal{F}_{i-1}]$, so $\mathbb{E}[(i^2 \mathbb{E}[\delta_i^2 \mid \mathcal{F}_{i-1}])^2] \leq i^4 \mathbb{E}[\delta_i^4] \leq C$ by Assumption 3. Hence $\{i^2 \mathbb{E}[\delta_i^2 \mid \mathcal{F}_{i-1}]\}$ is L^2 -bounded and therefore uniformly integrable, which allows taking expectations through the a.s. limit in Assumption 1: $\mathbb{E}[\delta_i^2] \leq (V(x) + 1)/i^2$ for all large i , and $\sum_{i \geq 1} \mathbb{E}[\delta_i^2] < \infty$. The martingale part $M_n = \sum_{i=1}^n \zeta_i$ is therefore L^2 -bounded. The bias part $B_n = \sum_{i=1}^n \xi_i$ converges absolutely in L^2 because $\sum_i \|\xi_i\|_2 \leq \sum_i \sqrt{i} \|\xi_i\|_2 < \infty$ by Assumption 2. Hence $(m_n(x))$ is L^2 -bounded and uniformly integrable, and $m_\infty(x) = m_0(x) + \sum_{i=1}^\infty \delta_i$ exists a.s.

(i) *Quasi-martingale condition with \sqrt{i} weights.* Theorem G.4 requires $\sum_{i \geq 1} \sqrt{i} \mathbb{E}[\|\xi_i\|] < \infty$. Since $\mathbb{E}[\|\xi_i\|] \leq \|\xi_i\|_2$ by Jensen's inequality, this follows immediately from Assumption 2.

(ii) *Supremum bound.* Since $(\sup_{i \geq 1} \sqrt{i} |\delta_i|)^4 \leq \sum_{i=1}^\infty i^2 \delta_i^4$, taking expectations and applying Assumption 3:

$$\mathbb{E} \left[\left(\sup_{i \geq 1} \sqrt{i} |\delta_i| \right)^4 \right] \leq \sum_{i=1}^\infty i^2 \mathbb{E}[\delta_i^4] \leq C \sum_{i=1}^\infty i^{-2} < \infty,$$

so $\sup_i \sqrt{i} |\delta_i| \in L^4 \subset L^1$, verifying condition (ii).

(iii) *A.s. variance convergence.* Apply Fortini et al. [10], Lemma G.5 with $W_i = i^2 \delta_i^2$. The two lemma conditions are: (a) $\sum_{i \geq 1} i^{-2} \mathbb{E}[W_i^2] = \sum_i i^2 \mathbb{E}[\delta_i^4] \leq C \sum_i i^{-2} < \infty$ by Assumption 3; (b) $\mathbb{E}[W_{i+1} \mid \mathcal{F}_i] = (i+1)^2 \mathbb{E}[\delta_{i+1}^2 \mid \mathcal{F}_i] \rightarrow V(x)$ a.s. by Assumption 1. The lemma then gives $n \sum_{i \geq n} W_i / i^2 = n \sum_{i \geq n} \delta_i^2 \rightarrow V(x)$ a.s., which is condition (iii).

All four requirements of Theorem G.4 are satisfied, giving $\mathcal{L}(\sqrt{n}(m_\infty(x) - m_n(x)) \mid \mathcal{D}_{1:n}) \xrightarrow{w} \mathcal{N}(0, V(x))$, \mathbb{P} -a.s.

Part 2: Consistency of $\hat{V}_{s_n}(x)$.

Write $D_j = M_j + R_j$ where $M_j = \sum_{i=t_{j-1}+1}^{t_j} \zeta_i$ and $R_j = \sum_{i=t_{j-1}+1}^{t_j} \xi_i$.

Step 2a: Block mean. Let $I_j = \{t_{j-1} + 1, \dots, t_j\}$. On the geometric grid, for all large j , $t_j/t_{j-1} \leq b$ and $t_j - t_{j-1} \geq c_b t_{j-1}$ for a constant $c_b > 0$. Hence $w_j = O(t_{j-1})$ and

$$\sum_{i \in I_j} i^{-2} = w_j^{-1} (1 + o(1)).$$

We first identify the total predictable second moment of the block. Put $A_i = i^2 \mathbb{E}[\delta_i^2 \mid \mathcal{F}_{i-1}]$. By Assumption 1, $A_i \rightarrow V(x)$ a.s.; by conditional Jensen and Assumption 3, $\{A_i^2\}$ is uniformly integrable. Thus $A_i \rightarrow V(x)$ in L^2 , and Toeplitz' lemma gives

$$w_j \sum_{i \in I_j} \frac{A_i}{i^2} \rightarrow V(x) \quad \text{in } L^2.$$

Taking expectations, this gives $w_j \sum_{i \in I_j} \mathbb{E}[\delta_i^2] \rightarrow V(x)$.

We now pass from the total increment δ_i to its martingale part. The decomposition $\delta_i = \zeta_i + \xi_i$ is orthogonal in L^2 , so $\mathbb{E}[\delta_i^2] = \mathbb{E}[\zeta_i^2] + \mathbb{E}[\xi_i^2]$. Let $T_j = \sum_{i \geq t_{j-1}} \sqrt{i} \|\xi_i\|_2$; by Assumption 2, $T_j \rightarrow 0$. Then

$$\|R_j\|_2 \leq \sum_{i \in I_j} \|\xi_i\|_2 \leq \frac{T_j}{\sqrt{t_{j-1}}}, \quad w_j \sum_{i \in I_j} \mathbb{E}[\xi_i^2] \leq \frac{w_j}{t_{j-1}} T_j^2 = o(1).$$

Consequently

$$w_j \mathbb{E}[M_j^2] = w_j \sum_{i \in I_j} \mathbb{E}[\zeta_i^2] = w_j \sum_{i \in I_j} \mathbb{E}[\delta_i^2] - w_j \sum_{i \in I_j} \mathbb{E}[\xi_i^2] \rightarrow V(x),$$

and $\|M_j\|_2 = O(w_j^{-1/2})$. Finally, expanding $D_j^2 = (M_j + R_j)^2$ shows that the remaining drift terms vanish:

$$2w_j \mathbb{E}[M_j R_j] \leq 2w_j \|M_j\|_2 \|R_j\|_2 = O(T_j) \rightarrow 0,$$

and $w_j \mathbb{E}[(R_j)^2] \leq (w_j/t_{j-1})T_j^2 = o(1)$. Therefore $w_j \mathbb{E}[D_j^2] \rightarrow V(x)$.

Step 2b: Second-moment bound for a single block. By the martingale Burkholder–Rosenthal inequality,

$$\mathbb{E}[M_j^4] \leq C_R \left(\mathbb{E} \left[\left(\sum_{i=t_{j-1}+1}^{t_j} \mathbb{E}[\zeta_i^2 \mid \mathcal{F}_{i-1}] \right)^2 \right] + \sum_{i=t_{j-1}+1}^{t_j} \mathbb{E}[\zeta_i^4] \right)$$

The predictable-variation term is $O(t_{j-1}^{-2})$ because $\mathbb{E}[\zeta_i^2 \mid \mathcal{F}_{i-1}] \leq \mathbb{E}[\delta_i^2 \mid \mathcal{F}_{i-1}]$ and the weighted block averages above are L^2 -bounded. The fourth-moment term is $O(t_{j-1}^{-3})$ by Assumption 3. Therefore $\mathbb{E}[M_j^4] = O(t_{j-1}^{-2})$. Since $w_j = O(t_{j-1})$, this gives $\mathbb{E}[(w_j M_j^2)^2] = O(1)$. Individual blocks do not concentrate to $V(x)$; averaging is essential.

Step 2c: Averaging over J blocks. We first remove the drift contribution in $D_j^2 = (M_j + R_j)^2$. Step 2a gives $w_j \mathbb{E}[M_j R_j] = O(T_j)$ and $w_j \mathbb{E}[(R_j)^2] = O(T_j^2)$, so Cesàro’s lemma gives

$$\frac{1}{J} \sum_{j=1}^J w_j (D_j^2 - M_j^2) \xrightarrow{L^1} 0.$$

It remains to average $w_j M_j^2$. Let

$$Y_j = \mathbb{E}[w_j M_j^2 \mid \mathcal{F}_{t_{j-1}}], \quad U_j = w_j M_j^2 - Y_j.$$

Then $\{U_j\}$ is a martingale difference sequence with respect to the block filtration $\{\mathcal{F}_{t_j}\}$. By Step 2b,

$$\mathbb{E} \left[\left(\frac{1}{J} \sum_{j=1}^J U_j \right)^2 \right] = \frac{1}{J^2} \sum_{j=1}^J \mathbb{E}[U_j^2] = O(1/J) \rightarrow 0.$$

Finally, we control the predictable part. Since martingale cross terms vanish conditionally,

$$Y_j = \mathbb{E} \left[w_j \sum_{i \in I_j} \mathbb{E}[\zeta_i^2 \mid \mathcal{F}_{i-1}] \mid \mathcal{F}_{t_{j-1}} \right].$$

Using $\mathbb{E}[\zeta_i^2 \mid \mathcal{F}_{i-1}] = A_i/i^2 - \xi_i^2$, the contraction property of conditional expectation, the L^2 convergence $w_j \sum_{i \in I_j} A_i/i^2 \rightarrow V(x)$, and the bound $w_j \sum_{i \in I_j} \mathbb{E}[\xi_i^2] \rightarrow 0$ from Step 2a, we obtain $Y_j \rightarrow V(x)$ in L^1 . Hence, again by Cesàro’s lemma,

$$\mathbb{E} \left[\left| \frac{1}{J} \sum_{j=1}^J (Y_j - V(x)) \right| \right] \rightarrow 0.$$

Combining the drift removal, martingale-difference average, and predictable average gives $\hat{V}_{s_n}(x) \xrightarrow{P} V(x)$. \square

Remark 3 (On the moment condition). *Assumption 3 is a convenient sufficient condition rather than a tight requirement. The CLT itself can be proved under weaker Lindeberg-type or maximal-increment conditions, and the variance-estimator argument mainly needs enough uniform integrability to control the weighted block squares $w_j D_j^2$. We state the stronger $4 + \epsilon$ moment condition because it gives a short proof of both requirements while keeping the theorem aligned with the predictive-CLT assumptions used above.*

A.2 Proof of Theorem 2

Proof. Construct PFN-TS and exact II-TS on the same probability space. They share the same draw $f_0 \sim \Pi$, the same context sequence, and the same reward noise whenever they select the same action. If their histories agree at the start of round t , couple their actions by a maximal coupling

of $Q_t(\cdot | X_t, \mathcal{D}_{t-1}^{(1:K)})$ and $P_t^\Pi(\cdot | X_t, \mathcal{D}_{t-1}^{(1:K)})$, where $\mathcal{D}_{t-1}^{(1:K)}$ denotes the collection of arm-specific histories. Then the conditional probability that their actions disagree is at most ε_t .

Let τ be the first round in which the coupled actions disagree, with $\tau = \infty$ if this never happens. If $\tau > t$, the two algorithms have identical histories and take the same action through round t . Thus

$$\Pr(\tau = t | \tau \geq t) \leq \varepsilon_t, \quad \Pr(\tau \leq t) \leq \sum_{s=1}^t \varepsilon_s.$$

The regret difference at round t is zero on $\{\tau > t\}$. On $\{\tau \leq t\}$, condition on the context, the two actions, and the combined arm-specific histories observed by the coupled algorithms before the reward at round t . The posterior expected reward-range condition in Theorem 2 gives

$$\mathbb{E}\left[|f_0(X_t, A_t^{\Pi\text{-TS}}) - f_0(X_t, A_t^{\text{PFN}})| \mid X_t, A_t^{\Pi\text{-TS}}, A_t^{\text{PFN}}, \mathcal{D}_{t-1}^{\text{cpl}}\right] \leq 2B_R,$$

where $\mathcal{D}_{t-1}^{\text{cpl}}$ denotes the combined histories generated by the coupled process. Hence

$$\mathbb{E}[\text{Regret}_T^{\text{PFN}}] \leq \mathbb{E}[\text{Regret}_T^{\Pi\text{-TS}}] + 2B_R \sum_{t=1}^T \Pr(\tau \leq t).$$

Using the previous union bound and exchanging the order of summation gives

$$\mathbb{E}[\text{Regret}_T^{\text{PFN}}] \leq \mathbb{E}[\text{Regret}_T^{\Pi\text{-TS}}] + 2B_R \sum_{t=1}^T \sum_{s=1}^t \varepsilon_s = \mathbb{E}[\text{Regret}_T^{\Pi\text{-TS}}] + 2B_R \sum_{s=1}^T (T - s + 1)\varepsilon_s.$$

□

Remark 4 (Information-gain bound for exact Π -TS). *The exact Bayesian term in Theorem 2 can be bounded by applying the standard information-ratio inequality to exact Π -TS:*

$$\mathbb{E}[\text{Regret}_T^{\Pi\text{-TS}}] \leq \sqrt{2T \bar{\Gamma}_T(\Pi) I_\Pi(f_0; \mathcal{H}_T^{\Pi\text{-TS}})}.$$

Under disjoint encoding and the product prior $\Pi = \bigotimes_{a=1}^K \Pi_a$, the information acquired across arms factorizes as

$$I_\Pi(f_0; \mathcal{H}_T) = \sum_{a=1}^K I_{\Pi_a}(f_0(\cdot, a); \mathcal{H}_{T,a}).$$

Consequently, $I_\Pi(f_0; \mathcal{H}_T^{\Pi\text{-TS}}) \leq \gamma_T(\Pi)$, where

$$\gamma_n(\Pi_a) = \sup_{x_1, \dots, x_n \in \mathcal{X}} I_{\Pi_a}(f_0(\cdot, a); (R_1, \dots, R_n) \mid X_i = x_i, A_i = a)$$

is the usual maximum information gain for arm a , and

$$\gamma_T(\Pi) = \max_{n_1 + \dots + n_K = T} \sum_{a=1}^K \gamma_{n_a}(\Pi_a).$$

If the posterior reward distributions under Π are uniformly sub-Gaussian with proxy σ_R^2 , finite-action Thompson Sampling information-ratio bounds suggest $\bar{\Gamma}_T(\Pi) \lesssim K\sigma_R^2$ [12]. We keep $\bar{\Gamma}_T(\Pi)$ explicit because this is a condition on Bayesian reward distributions, not merely on observation noise.

Proposition 3 (Sampler error from PPD approximation). *For each arm a , let $\mathcal{D}^{(a)}$ denote the arm-specific history used by disjoint encoding, let s_a be its latest refresh size, and write $\mathcal{D}_s^{(a)} = \mathcal{D}_{1:s_a}^{(a)}$. Let $m^\Pi(x; \mathcal{D}_s^{(a)})$ be the exact posterior predictive mean under Π , and let $m(x; \mathcal{D}_s^{(a)})$ be the predictive mean used by PFN-TS. Let $\hat{V}^\Pi(x; \mathcal{D}_s^{(a)})$ be the SubCLT variance estimate obtained by applying SubCLT to the exact Π -predictive mean sequence, and let $\hat{V}(x; \mathcal{D}_s^{(a)})$ be the SubCLT variance estimate from the TabICL predictive sequence. Assume these variance estimates are strictly*

positive; in applications this can be enforced by applying a common deterministic variance floor. For $\mathcal{D}^{(1:K)} = (\mathcal{D}^{(1)}, \dots, \mathcal{D}^{(K)})$, define

$$G_t^\Pi(x, \mathcal{D}^{(1:K)}) = \bigotimes_{a=1}^K \mathcal{N}\left(m^\Pi(x; \mathcal{D}_s^{(a)}), \frac{\hat{V}^\Pi(x; \mathcal{D}_s^{(a)})}{s_a}\right),$$

$$G_t(x, \mathcal{D}^{(1:K)}) = \bigotimes_{a=1}^K \mathcal{N}\left(m(x; \mathcal{D}_s^{(a)}), \frac{\hat{V}(x; \mathcal{D}_s^{(a)})}{s_a}\right).$$

Let $S_t^\Pi(\cdot | x, \mathcal{D}^{(1:K)})$ be the exact posterior sampling distribution over action-value vectors under Π . Suppose PFN-TS samples an action-value vector from $G_t(x, \mathcal{D}^{(1:K)})$ at round t , and let

$$\rho_t = \sup_{x, \mathcal{D}^{(1:K)}} \text{TV}\left(S_t^\Pi(\cdot | x, \mathcal{D}^{(1:K)}), G_t^\Pi(x, \mathcal{D}^{(1:K)})\right)$$

denote the uniform Gaussian approximation error for exact posterior sampling under Π , including the error from comparing exact full-history posterior sampling with the snapshot posterior at refresh sizes (s_1, \dots, s_K) . Define

$$\Delta_{t,a}(x, \mathcal{D}^{(a)}) = m(x; \mathcal{D}_s^{(a)}) - m^\Pi(x; \mathcal{D}_s^{(a)}), \quad r_{t,a}(x, \mathcal{D}^{(a)}) = \frac{\hat{V}(x; \mathcal{D}_s^{(a)})}{\hat{V}^\Pi(x; \mathcal{D}_s^{(a)})}.$$

Then

$$\varepsilon_t \leq \rho_t + \frac{1}{2} \sup_{x, \mathcal{D}^{(1:K)}} \left(\sum_{a=1}^K \left[r_{t,a}(x, \mathcal{D}^{(a)}) + \frac{s_a \Delta_{t,a}^2(x, \mathcal{D}^{(a)})}{\hat{V}^\Pi(x; \mathcal{D}_s^{(a)})} - 1 - \log r_{t,a}(x, \mathcal{D}^{(a)}) \right] \right)^{1/2}.$$

Proof of Theorem 3. The action is a measurable function of the sampled action-value vector, so data processing gives

$$\text{TV}\left(Q_t(\cdot | x, \mathcal{D}^{(1:K)}), P_t^\Pi(\cdot | x, \mathcal{D}^{(1:K)})\right) \leq \text{TV}\left(G_t(x, \mathcal{D}^{(1:K)}), S_t^\Pi(\cdot | x, \mathcal{D}^{(1:K)})\right).$$

By the triangle inequality for total variation,

$$\text{TV}(G_t, S_t^\Pi) \leq \text{TV}(G_t, G_t^\Pi) + \text{TV}(G_t^\Pi, S_t^\Pi),$$

where all terms are evaluated at a fixed $(x, \mathcal{D}^{(1:K)})$. The last term is bounded by ρ_t . It remains to bound the TV distance between the two diagonal Gaussians. By Pinsker's inequality and the KL divergence between diagonal Gaussians,

$$\begin{aligned} \text{TV}(G_t, G_t^\Pi) &\leq \sqrt{\frac{1}{2} \text{KL}(G_t \| G_t^\Pi)} \\ &= \frac{1}{2} \left(\sum_{a=1}^K \left[r_{t,a}(x, \mathcal{D}^{(a)}) + \frac{s_a \Delta_{t,a}^2(x, \mathcal{D}^{(a)})}{\hat{V}^\Pi(x; \mathcal{D}_s^{(a)})} - 1 - \log r_{t,a}(x, \mathcal{D}^{(a)}) \right] \right)^{1/2}. \end{aligned}$$

Taking the supremum gives Theorem 3. \square

Remark 5 (Interpreting the residual term). *The residual ρ_t is the Gaussian approximation error for exact posterior sampling under Π . When the predictive CLT gives a Berry–Esseen rate for the exact posterior, one expects $\rho_t = O(C_{\text{BE}}/\sqrt{s_{t,\min}})$, where $s_{t,\min} = \min_a s_{t,a}$ is the smallest refresh size, up to finite-grid SubCLT error computed with the exact Π -predictive sequence and any posterior-refresh error from using snapshot rather than full histories.*

Remark 6 (Variance error from predictive-mean paths). *The variance term in Theorem 3 can also be controlled by approximation error of the predictive means along the SubCLT grid. Let $t_0 < \dots < t_j$ be the grid for an arm history $\mathcal{D}^{(a)}$, and write*

$$D_j = m(x; \mathcal{D}_{1:t_j}^{(a)}) - m(x; \mathcal{D}_{1:t_{j-1}}^{(a)}), \quad D_j^\Pi = m^\Pi(x; \mathcal{D}_{1:t_j}^{(a)}) - m^\Pi(x; \mathcal{D}_{1:t_{j-1}}^{(a)}).$$

Algorithm 1 Subsampled CLT (SUBCLT)

Require: Model \mathcal{M} , history $\mathcal{D} = \{(x_i, r_i)\}_{i=1}^n$, query x , base $b > 1$; the grid below contains at least one block

- 1: Compute grid $G = \{2=t_0 < t_1 < \dots < t_J \leq n\}$ by iterating $t_{j+1} = \max(t_j+1, \lfloor bt_j \rfloor)$ while $t_{j+1} \leq n$
- 2: $m_0 \leftarrow m(x; \mathcal{D}_{1:2})$ ▷ forward pass on first 2 observations
- 3: **for** $j = 1, \dots, J$ **do**
- 4: $m_j \leftarrow m(x; \mathcal{D}_{1:t_j})$ ▷ forward pass, reuse cache from step $j-1$
- 5: $D_j \leftarrow m_j - m_{j-1}$
- 6: $w_j \leftarrow t_j t_{j-1} / (t_j - t_{j-1})$
- 7: **end for**
- 8: $\hat{V} \leftarrow \frac{1}{J} \sum_{j=1}^J w_j D_j^2$
- 9: **return** m_J, \hat{V}, t_J ▷ latest snapshot mean, variance, and size

If $\hat{V} = J^{-1} \sum_{j=1}^J w_j D_j^2$ and $\hat{V}^\Pi = J^{-1} \sum_{j=1}^J w_j (D_j^\Pi)^2$, then

$$|\hat{V} - \hat{V}^\Pi| \leq \frac{1}{J} \sum_{j=1}^J w_j |D_j - D_j^\Pi| (|D_j| + |D_j^\Pi|).$$

Moreover, with $e_i(x; \mathcal{D}^{(a)}) = |m(x; \mathcal{D}_{1:i}^{(a)}) - m^\Pi(x; \mathcal{D}_{1:i}^{(a)})|$,

$$|D_j - D_j^\Pi| \leq e_{t_j}(x; \mathcal{D}^{(a)}) + e_{t_{j-1}}(x; \mathcal{D}^{(a)}).$$

Thus the variance component is also controlled by TabICL’s approximation to the exact PPD predictive means, but along the full SubCLT prefix path rather than only at the final history.

Remark 7 (Interpreting the information gain). *The information gain $\gamma_T(\Pi)$ for the prior Π associated with TabICL is not explicitly characterized. It should be read as the Bayesian complexity of the exact prior model that PFN-TS is approximating. In contextual bandits, familiar examples give the following scales, suppressing constants and noise parameters. With K arms and d -dimensional linear rewards, the disjoint information gain is $\gamma_T = O(Kd \log T)$ [1, 25]. For squared-exponential kernel or Gaussian-process models in d dimensions, $\gamma_T = O(K(\log T)^{d+1})$ [16, 5]. For Matérn kernels with smoothness parameter ν , a common GP proxy for Sobolev/Hölder-type smoothness, the information gain is $\gamma_T = \tilde{O}(KT^{d/(2\nu+d)})$ [28]; heuristically, an α -Hölder class gives the analogous rate $\tilde{O}(KT^{d/(2\alpha+d)})$. For BART priors, the Bayesian regret bound of Deng et al. [6] is $O(K\sqrt{T} \log T)$, which corresponds to a logarithmic effective complexity term, of order $K \log T$ in the information-gain part of the bound, for the BART model class [4, 6].*

For TabICL and TabPFN, the prior Π is meant to cover a broad collection of tabular data-generating mechanisms rather than a single hand-specified class. Empirical evidence that TabPFN adapts across many simple and complex tabular regimes [31] suggests that the effective information gain of Π should also adapt to the structure revealed by the history. Thus, although a worst-case bound for the full prior could be loose, one expects $\gamma_T(\Pi)$ to behave more like the information gain of a simpler local model on easy instances, leading to regret closer to the \sqrt{T} rate when the realized reward functions have low effective complexity. Proving such an adaptive information-gain bound for PFN priors is left for future work.

B Algorithm details

B.1 Subsampled CLT

B.2 Full algorithm

B.3 Encoding selection and termination

At each switch time $s \in S$, the CRPS for all observations since the previous switch time is computed for both encodings by replaying observations against the cached model snapshots; this interval CRPS

Algorithm 2 PFN-TS

Require: Model \mathcal{M} , horizon T , arms K , base b , switch times $S = \{s_1 < \dots < s_L\}$, warm-up rounds τ , arm threshold K_{thr}

- 1: $e^* \leftarrow$ disjoint if $K < K_{\text{thr}}$, else one-hot; $e^\dagger \leftarrow$ the other encoding
- 2: $C \leftarrow 0, C^\dagger \leftarrow 0$; dual-caching \leftarrow **true**
- 3: **for** $t = 1, \dots, T$ **do**
- 4: Observe X_t
- 5: **if** $t \leq \tau K$ **then**
- 6: $A_t \leftarrow 1 + ((t - 1) \bmod K)$ \triangleright round-robin warm-up
- 7: **else**
- 8: **for** $k = 1, \dots, K$ **do**
- 9: $(\tilde{m}, \hat{V}, s_k) \leftarrow \text{SUBCLT}(\mathcal{M}, \mathcal{D}^{(k, e^*)}, X_t, b)$
- 10: $\tilde{r}_k \sim \mathcal{N}(\tilde{m}, \hat{V}/s_k)$
- 11: **end for**
- 12: $A_t \leftarrow \arg \max_k \tilde{r}_k$
- 13: **end if**
- 14: Observe R_t ; append (X_t, R_t) to active history $\mathcal{D}^{(A_t, e^*)}$
- 15: **if** dual-caching **then**
- 16: Also append (X_t, R_t) to challenger history $\mathcal{D}^{(A_t, e^\dagger)}$; extend challenger snapshot cache if arm grid point reached
- 17: **end if**
- 18: **if** $t \in S$ **then**
- 19: Score all obs since last switch for each encoding using cached snapshots; add interval CRPS to C, C^\dagger respectively
- 20: **if** $C^\dagger < C$ **then**
- 21: Swap $e^* \leftrightarrow e^\dagger$; swap all caches and histories; swap $C \leftrightarrow C^\dagger$
- 22: **end if**
- 23: **if** $t = s_L$ **then**
- 24: dual-caching \leftarrow **false**; discard challenger caches
- 25: **end if**
- 26: **end if**
- 27: **end for**

is added to the respective cumulative totals C and C^\dagger . The encoding with lower cumulative CRPS becomes the active encoding. Dual caching terminates unconditionally at the last switch time s_L (default $s_L = 2048$), after which only the active encoding’s caches are retained and the challenger is discarded. No additional forward passes are required for CRPS scoring since the snapshot caches built during Thompson Sampling are reused.

B.4 CRPS computation

For TabICL’s discretized output distribution (a probability mass function over binned response values), CRPS is computed exactly as a sum over the bin CDF:

$$\text{CRPS}(\hat{F}, r) = \sum_j (\hat{F}(y_j) - \mathbf{1}\{y_j \geq r\})^2 \Delta y_j,$$

where y_j are the bin midpoints and Δy_j are the bin widths. This is computed at zero additional forward-pass cost since \hat{F} is already available from the prediction step.

B.5 Caching in TabICL

TabICL caches the key-value representations for a fixed training set $\mathcal{D}_{1:t_j}$ after computing $\mu_{t_j}(x)$. Because the grid is evaluated in increasing order, the cache from step $j - 1$ can be extended to step j by appending the new observations $\mathcal{D}_{t_{j-1}+1:t_j}$ and recomputing only the affected attention layers. This reduces the per-step cost from $O(t_j^2)$ to $O((t_j - t_{j-1}) \cdot t_j)$, a substantial saving on the coarser geometric grid.

C Experimental Specifications

All experiments use global random seed 42, with per-replication seeds derived from it.

Compute environment. PFN-TS used an NVIDIA RTX 5090 GPU for the synthetic experiments, ablation studies, and coverage analysis, and an NVIDIA RTX PRO 6000 GPU with 96 GB of memory for the OpenML experiments. On each dataset, wall-clock time for a $T = 10,000$ horizon is a few hours. NeuralTS [32] used an NVIDIA A40 GPU and one 36-core CPU socket. All other baselines ran on CPU with 4 logical cores. BFTS used 4 parallel MCMC chains, and RFTS and XGBoostTS (TETS-RF and TETS-XGBoost in 21) used OpenMP parallelization with `nthread=4`. Because hardware and parallelization differed across methods, we do not report detailed wall-clock runtime comparisons.

C.1 Synthetic DGP Specifications

All synthetic experiments use horizon $T = 10,000$ and $R = 5$ independent replications. The interaction proceeds at each round $t = 1, \dots, T$ as follows: a context $X_t \in \mathbb{R}^P$ arrives, the agent selects arm $a_t \in \{1, \dots, K\}$, and observes reward $Y_t = \mu_{a_t}(X_t) + \varepsilon_t$ with independent noise. Unless stated otherwise, $\varepsilon_t \sim \mathcal{N}(0, \sigma^2)$.

Linear ($P = 10, K = 3$). Contexts are i.i.d. $X_t \sim \text{Unif}([0, 1]^P)$. For each arm a , coefficients $\beta_a \in \mathbb{R}^P$ are drawn with $\beta_{a,j} \stackrel{\text{iid}}{\sim} \mathcal{N}(0, 1)$. The mean reward is $\mu_a(x) = \beta_a^\top x$.

Friedman variants ($P \in \{5, 20\}, K = 2$). Contexts are i.i.d. $X_t \sim \text{Unif}([0, 1]^P)$. The base Friedman1 function is

$$f(x_1, \dots, x_5) = 10 \sin(\pi x_1 x_2) + 20(x_3 - 0.5)^2 + 10x_4 + 5x_5.$$

For FRIEDMAN2 and FRIEDMAN3, the first four coordinates are rescaled as $x'_1 = 100x_1, x'_2 = 40\pi + 520\pi x_2, x'_3 = x_3, x'_4 = 1 + 10x_4$, with

$$f_2(x) = \frac{1}{125} \sqrt{(x'_1)^2 + (x'_2 x'_3 - (x'_2 x'_4)^{-1})^2}, \quad f_3(x) = \frac{1}{0.1} \arctan\left(\frac{x'_2 x'_3 - (x'_2 x'_4)^{-1}}{x'_1}\right).$$

Arm 1 uses the scenario-specific function (f, f_2 , or f_3). Arm 2 uses a *shared* variant $\mu_2(x) = f(x_1, \dots, x_5) + 5 \sin(\pi x_1 x_2)$, or a *disjoint* variant $\mu_2(x) = f(x_P, x_{P-1}, \dots, x_1)$ (reversed feature order). Sparse variants increase context dimensionality to $P = 20$ while keeping the reward functions low-dimensional.

Friedman-Heteroscedastic. Same mean functions as the shared Friedman variant, with arm-specific noise: for each arm a , $\sigma_a^2 = 10^{U_a}$ where $U_a \sim \text{Unif}(-1, 1)$ is drawn once per replication.

SynBART ($P = 4, K = 3$). Contexts are i.i.d. $X_t \sim \text{Unif}([0, 1]^P)$. Each arm’s mean reward function $\mu_a(\cdot)$ is sampled from a BART prior [4] with $m = 100$ trees, depth-geometric splitting prior with $\alpha = 0.45$, Gaussian leaf prior with $\kappa = 2$, and Dirichlet-sparse split probabilities with $(\zeta, \xi) = (1, 1)$. Noise variance is fixed to $\sigma^2 = 0.01$. This DGP is correctly specified for BFTS and represents a challenging nonlinear benchmark for methods with a different prior.

C.2 OpenML Dataset Details

We evaluate on eight OpenML classification datasets: Adult, Coverttype, EEGEyeState, GasDrift, MagicTelescope, Mushroom, PageBlocks, and Shuttle. Each dataset defines a contextual bandit: the feature vector is the context, each class label is an arm, and the reward is 1 for selecting the true class and 0 otherwise. We follow the preprocessing of Zhang et al. [32], Deng et al. [6]: features are standardized, categorical variables are one-hot encoded, and the interaction horizon is capped at $T = 10,000$ (or the dataset size if smaller; Mushroom has 8,124 rows). LinTS and NeuralTS hyperparameters are selected on a separate low-budget pilot run (one replication with a different seed) to avoid post-hoc tuning.

Remark 8. *Pilot tuning gives LinTS and NeuralTS a limited offline tuning budget relative to a strictly online setting. PFN-TS uses the same default settings across datasets.*

C.3 Drink Less Data Processing

The Drink Less data come from a micro-randomized trial (MRT) [2] involving $n = 349$ participants over 30 days. At 8:00 p.m. daily (local time), participants were randomized among three push-notification actions with static propensities (0.4, 0.3, 0.3): (i) no message, (ii) a standard message, and (iii) a message drawn from a bank of tailored variants. The binary reward $R_{i,d} \in \{0, 1\}$ indicates proximal engagement: whether participant i opened the app within one hour of the 8 p.m. decision point on day d .

The panel $\{(X_{i,d}, A_{i,d}, R_{i,d})\}$ is unfolded into a sequential stream of $T = 349 \times 30 = 10,470$ decision points, ordered by day d within each participant i and then interleaved across participants. This ordering preserves within-participant temporal structure while allowing sequential simulation of adaptive algorithms. The context X_t includes static participant covariates (AUDIT_score, age, gender, employment_type), the time-varying covariate days_since_download, and a one-hot user identifier to capture individual fixed effects. Features are standardized prior to bandit simulation.

OPE methodology. Since the algorithms cannot be deployed prospectively, we use offline replay-style sequential simulation [18]: at each step t , the algorithm proposes an action and is updated only if its proposal matches the logged action A_t , effectively using the logged data as an unbiased estimator of the interactive bandit environment under the logging propensities. Policy value is estimated via self-normalized importance sampling (SNIPS; Swaminathan and Joachims [26]):

$$\widehat{V}_{\text{SNIPS}}(\pi) = \frac{\sum_t w_t(\pi) R_t}{\sum_t w_t(\pi)}, \quad w_t(\pi) = \frac{\pi(A_t | X_t)}{\pi_0(A_t)},$$

where $\pi_0(a) \in \{0.4, 0.3, 0.3\}$ are the known logging propensities. Uncertainty is quantified via a user-level cluster bootstrap with $B = 30$ replicates. A doubly-robust (DR) estimator [7] is provided as a robustness check (see Section D.4).

Since the logging propensities are bounded away from zero, importance weights are bounded by $1/\min_a \pi_0(a) = 10/3$, ruling out severe positivity violations. Weight diagnostics are reported in Section D.4.

C.4 Hyperparameter Settings

PFN-TS. Unless stated otherwise in the ablation studies, PFN-TS uses the following defaults across all experiments:

- **Subsampling base:** $b = 2$ (geometric grid).
- **Context window:** no truncation; the full observed history for the relevant arm/encoding is retained.
- **Warm-up:** $\tau = 5$ round-robin pulls per arm before Thompson sampling.
- **Backbone model:** TabICL [22] with KV-cache enabled for the fixed training set per arm.
- **Encoding:** adaptive (disjoint for $n \leq N_{\text{thr}}$, joint otherwise, with $N_{\text{thr}} = 128$).

Baselines. Baseline implementations and fixed settings follow Deng et al. [6] unless noted below.

- **LinTS:** exploration parameter ν tuned from $\{1.0, 0.1, 0.01\}$ on a pilot run; $\lambda = 1$ (fixed).
- **LinUCB:** exploration parameter $\alpha = 1$ (fixed).
- **NeuralTS:** λ tuned from $\{1, 0.1, 0.01, 0.001\}$ and ν from $\{0.1, 0.01, 0.001, 0.0001\}$ on a pilot run.
- **BFTS:** default settings of [6] with $m = 100$ trees per arm, depth-exponential prior with $\alpha = 0.45$, Dirichlet-sparse split probabilities, $n_{\text{post}} = 500$, $n_{\text{burn}} = 500$, 4 chains, logarithmic refresh schedule, and the $\tau = 5$ warm-up convention.
- **RFTS, XGBoostTS:** default settings of Nilsson et al. [21] with $\nu = 1$ (fixed).

D Additional Experimental Results

D.1 Full Synthetic Regret Curves

Figure 6 provides cumulative regret trajectories across all synthetic scenarios described in Section C.1.

D.2 SubCLT Coverage Diagnostics

To isolate the quality of the SubCLT approximation from adaptive data collection, we run offline regression diagnostics on the Linear and Friedman DGPs. The DGPs match those in Section C.1, but the bandit structure is removed: we treat each arm in isolation and evaluate coverage on arm 0 only (Linear: $P = 10$, $\sigma^2 = 1$; Friedman: $P = 5$, Friedman1 variant with shared correlation, $\sigma^2 = 1$). For each DGP, training size $n \in \{16, 64, 256, 1024\}$, and replication, we independently resample the DGP parameters, training set, and 50 held-out query points. Coverage is evaluated for the latent mean reward $f_0(x)$, not for a noisy reward draw.

TabICL-SubCLT forms nominal 95% intervals from the predictive-sequence approximation $\mathcal{N}(m_{s_n}(x), \hat{V}_{s_n}(x)/s_n)$ with geometric base $b = 2$. For comparison, BART intervals are computed from 500 posterior draws ($m = 100$ trees, $n_{\text{post}} = 500$, $n_{\text{burn}} = 500$, $\alpha = 0.95$, $\beta = 2.0$)—note that we use the default BART prior of Chipman et al. with their recommended settings, which differs from the BFTS choices in Section C.4. Figure 3 reports empirical coverage and mean interval length, averaged over 10 replications and 50 query points per replication.

D.3 Full OpenML Results

Figure 7 provides cumulative regret trajectories across all eight OpenML datasets.

D.4 OPE Diagnostics

Importance weight diagnostics. Under the static logging propensities $(0.4, 0.3, 0.3)$, importance weights are bounded by $1/\min_a \pi_0(a) = 10/3$. Figure 8 (left) shows the empirical weight distribution; weights remain close to their maximum, confirming that positivity violations are not a concern and SNIPS variance is well controlled.

Doubly-robust estimates. For each bootstrap replicate, a per-arm ridge outcome model $\hat{q}(x, a)$ is fit via 2-fold cross-fitting and used to form the DR estimate

$$\hat{V}_{\text{DR}}(\pi) = \frac{1}{n} \sum_{i=1}^n \left[\sum_a \pi(a | x_i) \hat{q}(x_i, a) + w_i (r_i - \hat{q}(x_i, a_i)) \right].$$

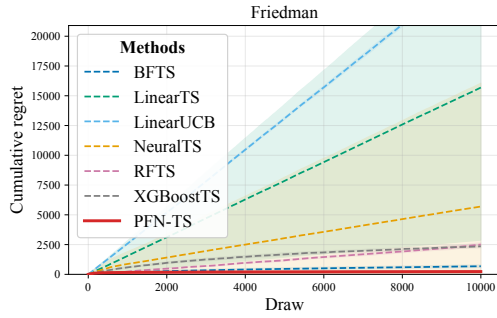
Figure 8 (right) shows the DR policy value curve over the horizon; the pattern closely tracks the SNIPS estimates, confirming robustness to the choice of estimator.

D.5 Ablation Plots

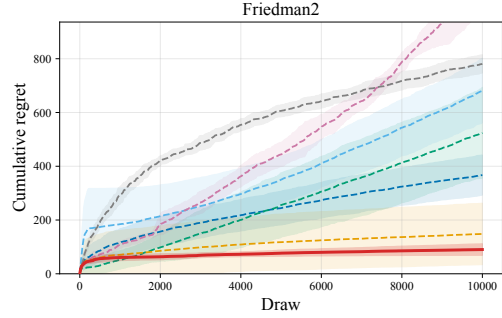
Encoding strategy. Figure 10 compares PFN-TS (adaptive), PFN-TS-Disjoint (fixed separate model), and PFN-TS-Joint (arm index concatenated to context) across synthetic and OpenML scenarios.

Subsampling grid. Figure 11 compares PFN-TS with geometric base $b \in \{1.5, 2, 3\}$ across the synthetic scenarios.

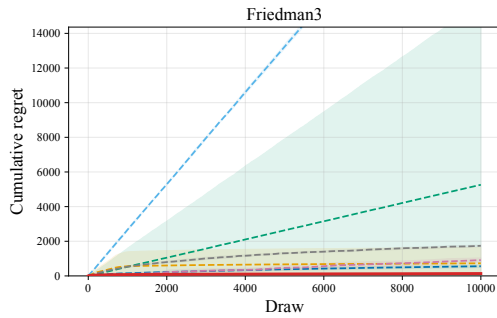
Decision rule. Figure 12 compares Thompson sampling (PFN-TS), posterior predictive sampling (PFN-PS), and a greedy baseline (highest predictive mean only).



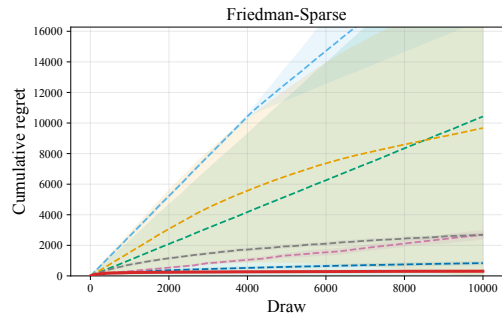
(a) Friedman



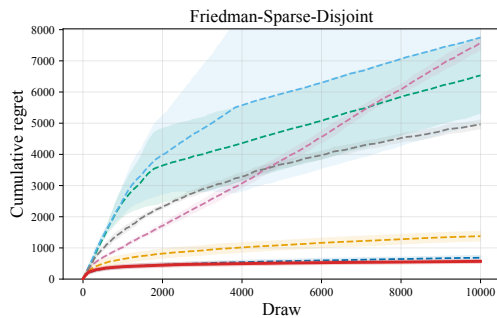
(b) Friedman2



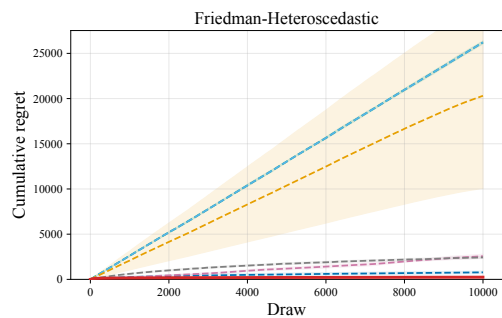
(c) Friedman3



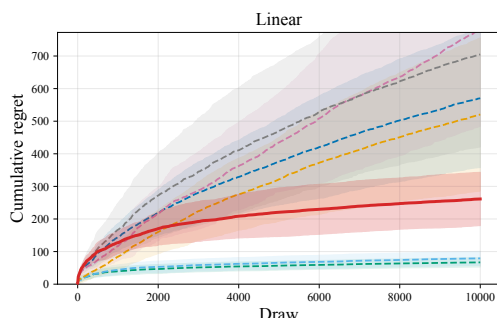
(d) Friedman-Sparse



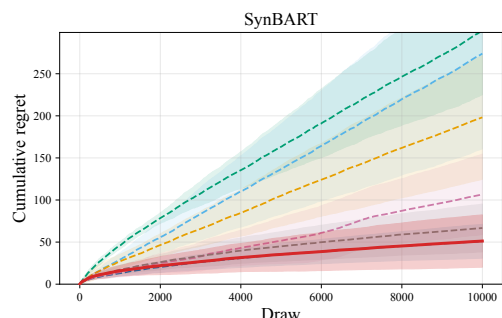
(e) Friedman-Sparse-Disjoint



(f) Friedman-Heteroscedastic



(g) Linear



(h) SynBART

Figure 6: Cumulative regret trajectories across all synthetic scenarios (mean \pm SD, $R = 5$ replications, $T = 10,000$).

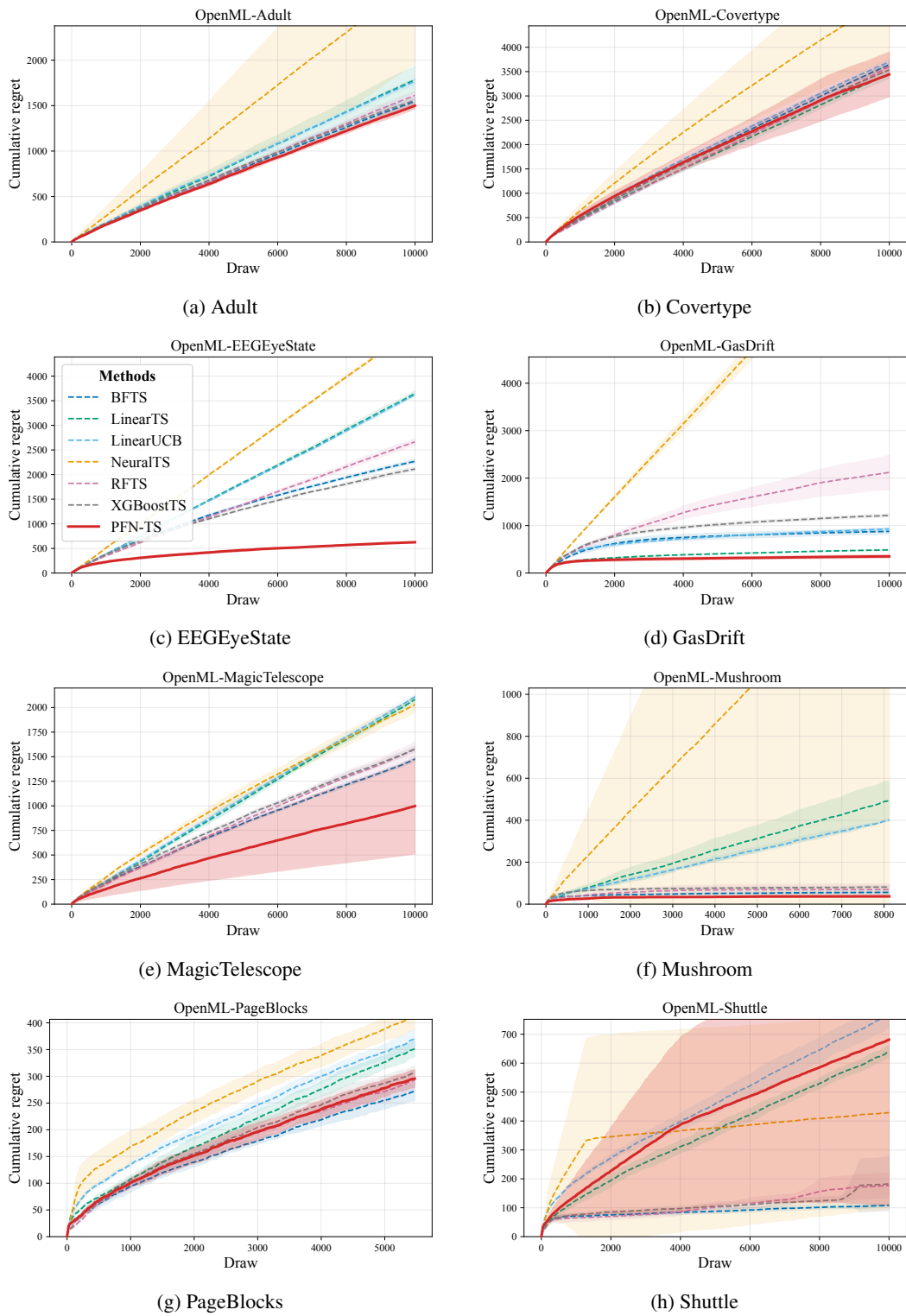


Figure 7: Cumulative regret trajectories on all eight OpenML datasets (mean \pm SD, $R = 5$ replications).

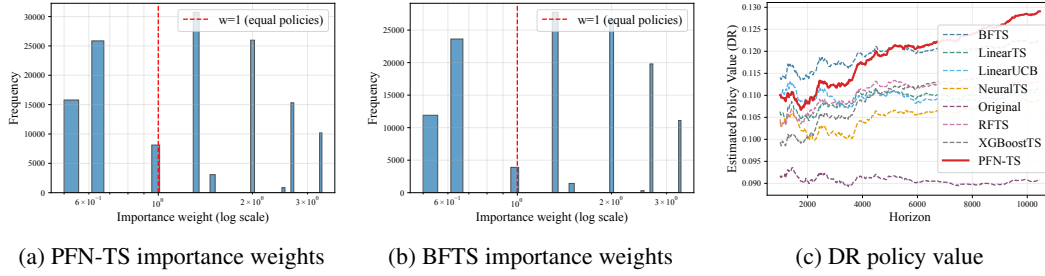


Figure 8: Drink Less OPE diagnostics. Left/centre: empirical importance weight distributions for PFN-TS and BFTS (log scale); weights are bounded by $10/3$ under the logging propensities, confirming no positivity violations. Right: policy value estimated via the doubly-robust estimator; the trajectory closely tracks the SNIPS estimates in Figure 4, confirming robustness to the choice of OPE estimator.

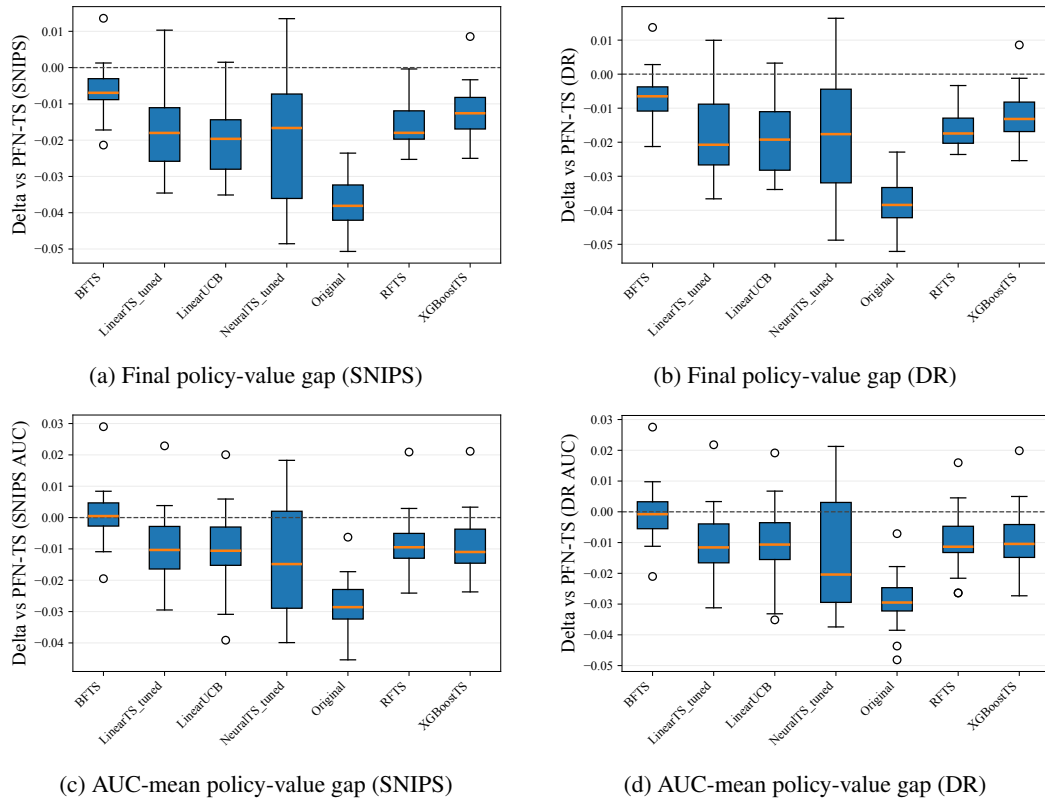


Figure 9: Bootstrap distributions ($B = 30$ user-level cluster replicates) of the policy-value gap between each method and the best-performing baseline, on the Drink Less trial. Top: gap at the final horizon $T = 10,470$. Bottom: gap integrated over the full horizon (AUC mean). Positive values indicate that the method outperforms the best baseline.

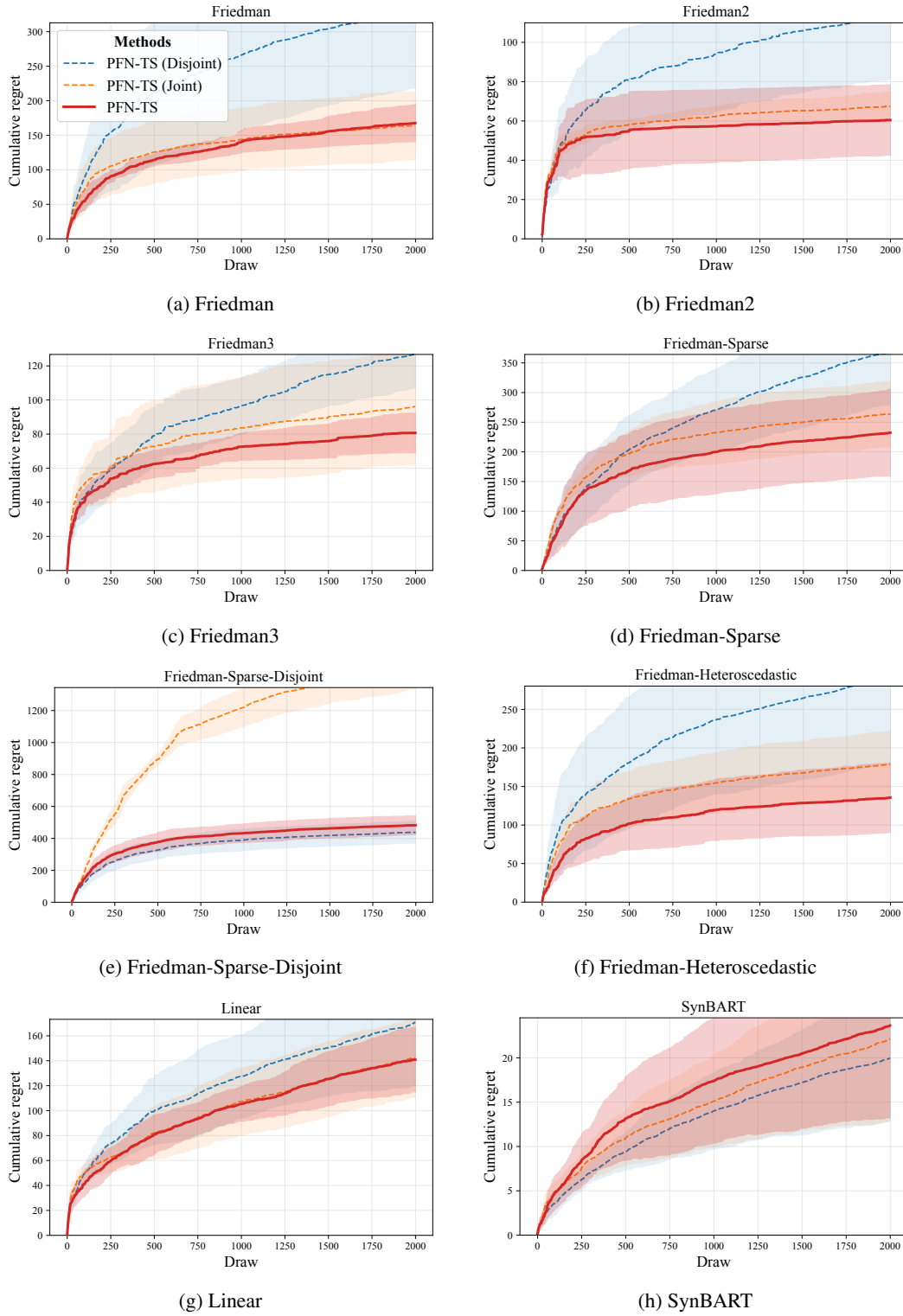


Figure 10: Encoding ablation: cumulative regret trajectories comparing the adaptive encoding rule against *Disjoint* (separate context per arm) and *Joint* (arm index appended to context) across all synthetic scenarios (mean \pm SD, $R = 5$ replications).

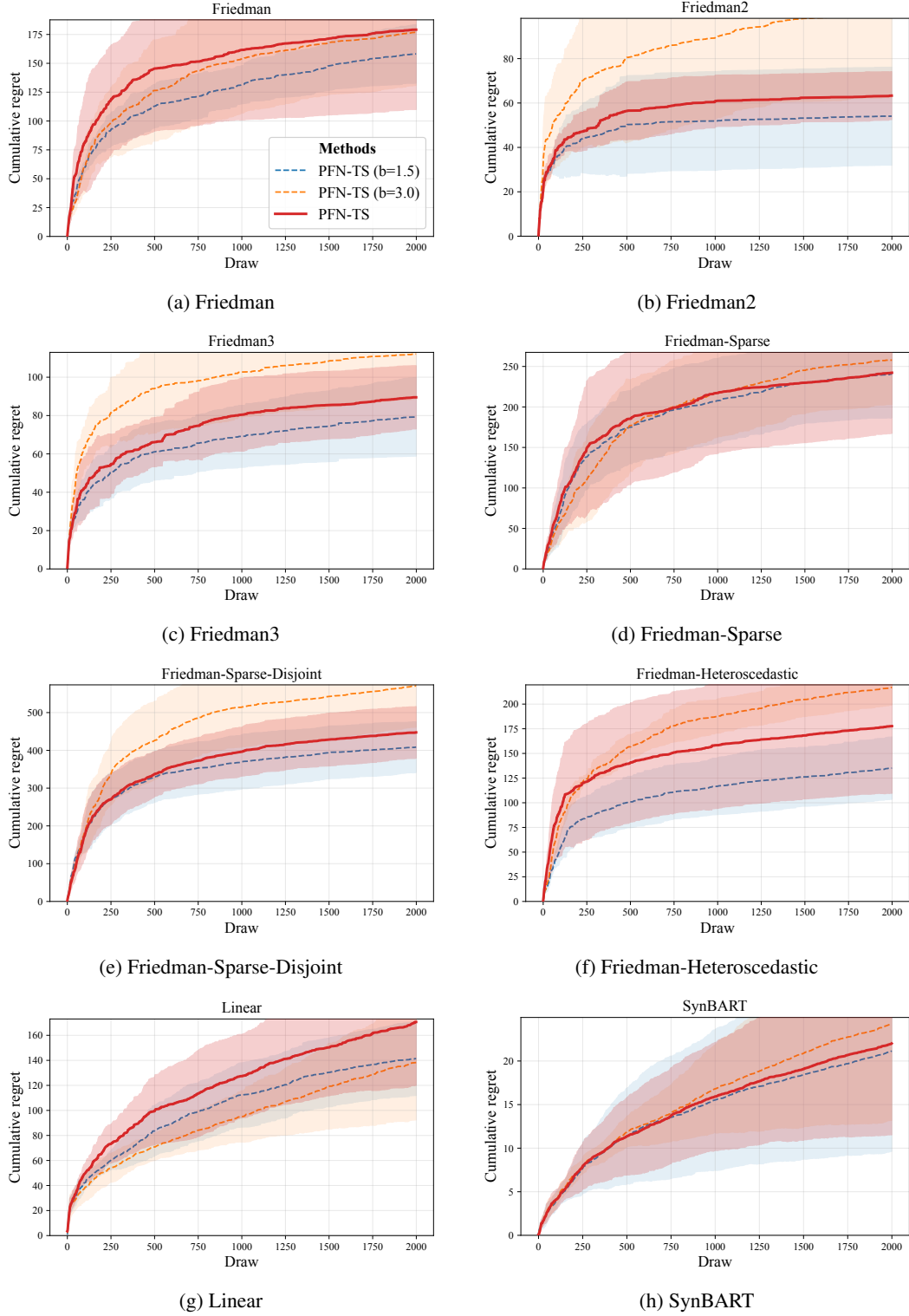


Figure 11: Subsampling grid ablation: cumulative regret trajectories for geometric base $b \in \{1.5, 2, 3\}$ across all synthetic scenarios (mean \pm SD, $R = 5$ replications).

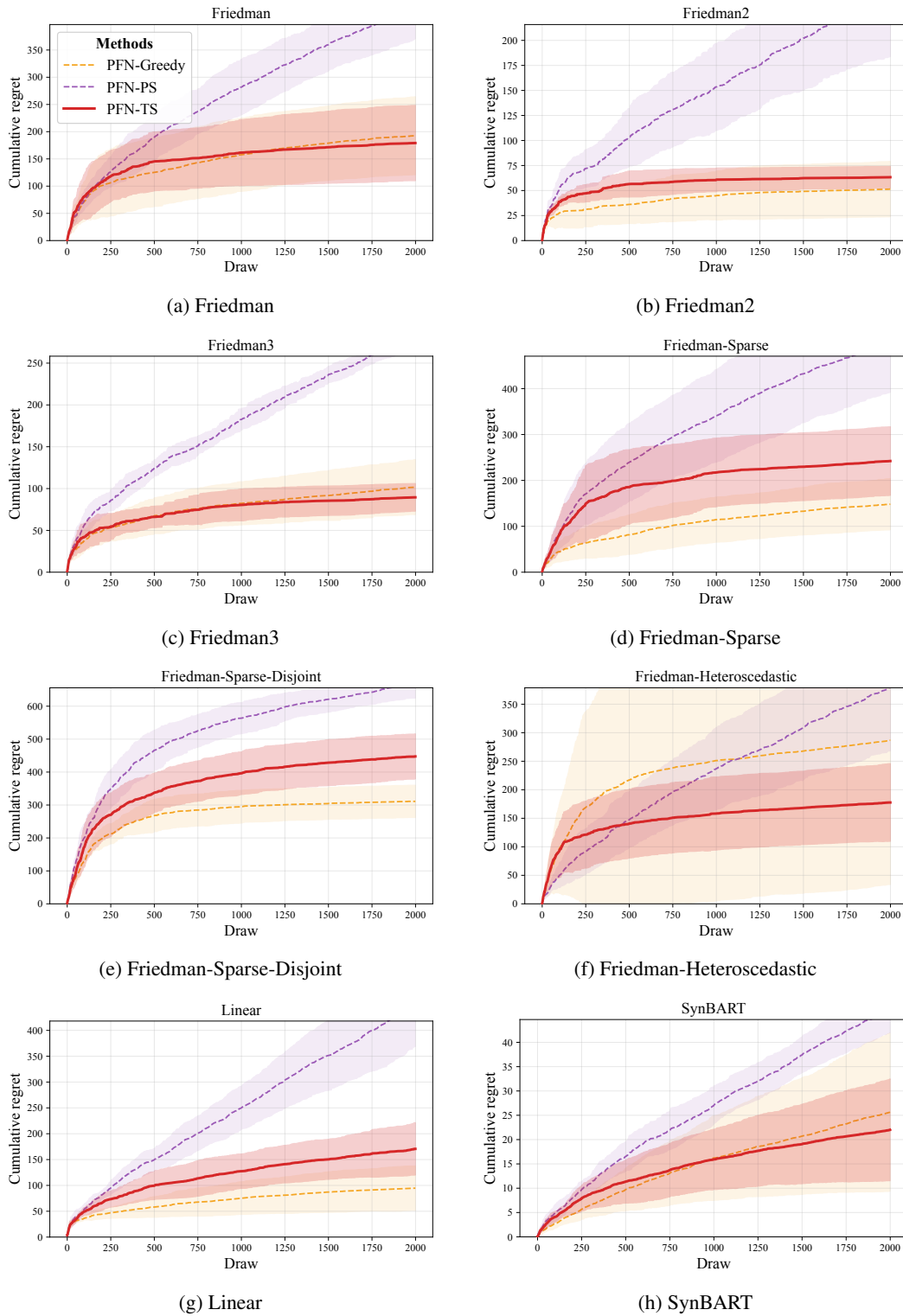
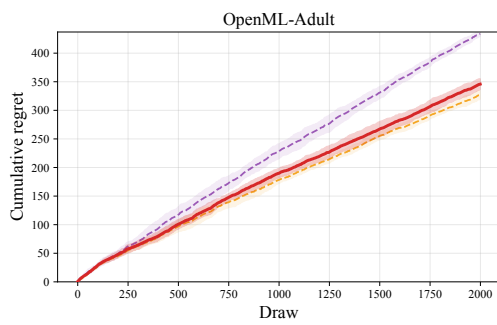
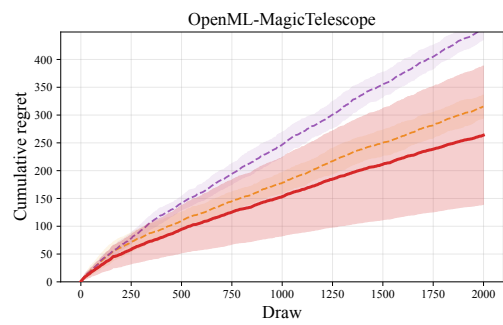


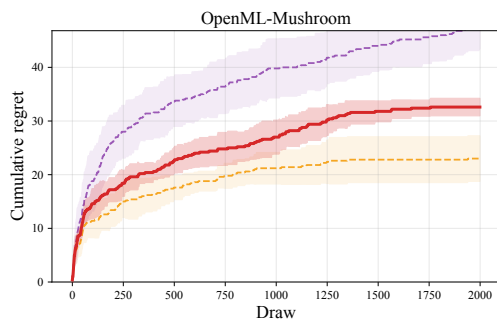
Figure 12: Decision rule ablation: cumulative regret trajectories comparing Thompson sampling (PFN-TS), PFN-PS, and greedy across synthetic scenarios (mean \pm SD, $R = 5$ replications). Continued in Figure 13.



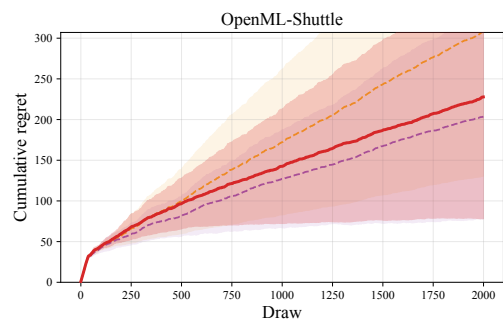
(a) Adult



(b) MagicTelescope



(c) Mushroom



(d) Shuttle

Figure 13: Decision rule ablation (OpenML scenarios, continued from Figure 12).